Marine Geology 408 (2019) 48–66

Contents lists available at ScienceDirect

Marine Geology

journal homepage: www.elsevier.com/locate/margo

A 2000 year geomagnetic field record from the Gulf of Papua

Rachel Marcuson*,[1], Jeffrey Gee, Emily Wei, Neal Driscoll

Scripps Institution of Oceanography, La Jolla, CA 92093-0220, USA

ARTICLE INFO

Editor: Michele Rebesco

Keywords:
Paleomagnetism
Holocene
Clinoform

ABSTRACT

A high resolution Holocene record of geomagnetic field direction and intensity in the Gulf of Papua was constructed using paleomagnetic data from eight piston cores collected in the region. The chronology of the cores was based largely on radiocarbon dates from benthic foraminifera. Correlation of seismic reflectors imaged in subbottom data between nearby cores was consistent with the chronostratigraphic framework based on radiocarbon dates and provided additional confidence of the age model. In other regions, where cores sampled different depositional settings associated with the three-dimensional prograding lobes, reflectors could not be confidently correlated between cores. Furthermore, radiocarbon ages from the bottoms of trigger cores and tops of co-located piston cores revealed varying amounts of overpenetration of the piston core below the seafloor. The relative paleointensity, and a general eastward trend in the declination and steepening of the inclination in our new record are generally compatible with the closest (> 4300 km) existing records. Our record does not agree well with global field models CALS3k and pfm9k, likely reflecting the lack of existing data contributing to field models in the region.

1. Introduction

Sediment records are key contributors to our knowledge of the global variability of the geomagnetic field. For the past 50 years sediments have proven to be useful recorders of magnetic field direction (e.g., Harrison and Somayajulu, 1966; Opdyke and Henry, 1969; Mackereth, 1971) and relative intensity (e.g., Levi and Banerjee, 1976; King et al., 1983; Tauxe, 1993). In addition, deep sea sediment sequences have been successfully used to construct long term (a few million years) records of relative paleointensity (dipole strength) (e.g., Ziegler et al., 2011; Channell et al., 2009; Valet et al., 2005) and to recognize excursions or polarity reversals in marine sequences (e.g., Clement and Kent, 1987; Ohneiser et al., 2013; Wu et al., 2014). Similarities between various regional stacks (e.g., Barletta et al., 2010b; Stoner et al., 2002; Yamamoto et al., 2007) and consistency with ^{10}Be records (Christl et al., 2003) provide increasing confidence in the reliability of these sedimentary records. High accumulation rate sediment records can also provide information on directional and intensity variations over shorter time scales that are used to construct Holocene global field models (e.g., Korte and Constable, 2011; Nilsson et al., 2014). These models aim to analyze global and regional field variations and provide insight into the dynamics of the core. Records with high sediment accumulation rates are preferred over those with lower rates, and the ideal data for these models will have measures of geomagnetic inclination, declination and intensity.

Holocene field models are based primarily on archeomagnetic data and high accumulation rate sedimentary records from lakes, as relatively few deep-sea sedimentary records have the required time resolution. Sedimentation rates in the open ocean are typically low (up to 5 cm/kyr for carbonate (Milliman, 1993), up to 1 cm/kyr for biogenic silica (Nelson et al., 1995), and < 0.5 cm/kyr for pelagic clays (Zhou and Kyte, 1992)) and provide insufficient temporal resolution to record the Holocene geomagnetic field with much detail. Continental margin sediments offer the possibility of obtaining high-resolution Holocene records and studies have been conducted in the Arctic (Barletta et al., 2008; Barletta et al., 2010b, Lisé-Pronovost et al., 2009), North Atlantic (Stoner et al., 2007) and Antarctic (Brachfeld et al., 2000). The current distribution of marine and lacustrine Holocene paleomagnetic sediment records is heavily biased towards the northern hemisphere and Europe, with very few records in the southern hemisphere (e.g., Nilsson et al., 2014), and fewer than 100 records globally. Continental margin sediments can potentially expand this sparse global coverage of Holocene records for paleomagnetic studies, but the more complex sedimentary environments of margins compared to lakes requires more scrutiny while correlating multiple cores. These complexities can include variations in accumulation rates that may differ by an order of magnitude

* Corresponding author at: Scripps Institution of Oceanography, La Jolla, CA 92093-0220, USA.
E-mail address: rmarcuson@usgs.gov (R. Marcuson).
[1] Present Address: U.S.G.S. Pacific Coastal and Marine Science Center, Santa Cruz, CA 95060, USA

https://doi.org/10.1016/j.margeo.2018.11.014
Received 4 October 2017; Received in revised form 1 November 2018; Accepted 20 November 2018
Available online 22 November 2018
0025-3227/ Published by Elsevier B.V.

over small spatial scales and hiatuses that can introduce data gaps.

The reliability of sedimentary geomagnetic records can be enhanced by using multiple local records. If there are sufficient age constraints on each core, combining the geomagnetic records from multiple cores at a single location into a single record can average out some of the variability in the sedimentary recording process. In practice, independent age constraints are not always available for each core and a composite record may be constructed by matching peaks in magnetic susceptibility (e.g., Gogorza et al., 2002; Constable and McElhinny, 1985) or by matching features in the inclination and declination (e.g., Lund et al., 2016). Both of these approaches may present challenges; magnetic susceptibility variations may be too small to identify correlatable features, and remanence directions may have spurious features that should not be used for correlation. Additionally, the justification for using either remanence or susceptibility variations for correlation is based on the assumption that variations must represent the same time period. Whether this is true depends on the spatial scale over which the correlation is made as well as variation in accumulation rates. For this reason, it is important to use independent (not related to magnetics) ways to establish correlation between cores. Some examples of lithologic features that characterize units that can be identified in each core are color changes (Verosub et al., 1986) representing oxic and anoxic sediments (Frank et al., 2007), rapidly deposited layers (Turner et al., 2015), and dated tephra layers (Ali et al., 1999). Radiocarbon dating, of wood, shells and foraminifera can be used to establish an age model, as can ^{210}Pb, which can be used to determine the sediment accumulation rates in cores, and environmental markers such as pollen that can help identify known, dated horizons (Brachfeld and Banerjee, 2000).

In this study, we examine the feasibility of using sediments from margins with very high sedimentation rates to get a high resolution, late Holocene field record from the continental margin of Papua New Guinea. Generating a composite record from the Gulf of Papua is challenging due to the complexity of the margin (Walsh et al., 2004; Harris et al., 1993; Slingerland et al., 2008a, 2008b), so we explore whether using seismic reflectors can help in establishing correlations between cores. The Gulf of Papua offers a distinct advantage for this test of using seismic reflectors because it was the focus of a multidisciplinary effort to understand source to sink properties of margin environments and, as a result, over 6800 km of seismic data (Slingerland et al., 2008a, 2008b), as well as fifty piston and gravity cores with companion trigger cores were collected. This site also represents a location where there is a distinct lack of recent paleomagnetic data. Although there are some nearby study sites, few cover the last 2000 years with good resolution. Constable (1985) and Constable and McElhinny (1985) studied two lakes in northeastern Australia, about 600 km away, but these lake sediments are missing approximately the last 1500 years. Lund et al. (2006) studied four cores from a transect in the western Equatorial Pacific Ocean but these too are missing the most recent Holocene, as are the box cores from the Ontong-Java Plateau measured by Constable and Tauxe (1987). More complete records were established by Richter et al. (2006), who provided a high resolution (400 cm/kyr) inclination and relative paleointensity record from the Western Pacific, and the Haberzettl et al. (2013) study of relative paleointensity and paleosecular variation for the past 1300 years in an Indonesian Lake (up to 900 cm/kyr sedimentation rate). The next closest southern hemisphere Holocene records that span 0–2000 years are found about 4000 km away in southern Australia (Barton and McElhinny, 1981) and New Zealand (Turner and Lillis, 1994; Turner et al., 2015).

Here we present a high-resolution composite record of geomagnetic field variations over the last 2000 years that included measurements from cores with accumulation rates up to 500 cm/kyr. The addition of this new record from the Gulf of Papua should complement existing studies and enhance our understanding of regional field variations in this area, specifically addressing whether the large inclination variations (~30° in 500 years) predicted by the CALS3k.4 (Korte and Constable, 2011) model are representative of this site, or whether those variations are due to the lack of regional data. Seismic and core data help constrain the offsets between trigger and piston cores. Local correlations between cores are consistent with radiocarbon data; however, regional seismic correlation is difficult along the Papua New Guinea margin because of the numerous river inputs.

2. Regional setting

The setting for this study is the Gulf of Papua, located off the southeast coast of Papua New Guinea (Fig. 1). This tropical region receives 2–9 m of rain per year (Harris et al., 1993). As a result, 3.84×10^8 tons (Milliman et al., 1999) of sediment is delivered to the gulf each year, with half of that transported mainly through three rivers, the Fly River in the south, and the Kikori and Purari rivers in the north (Milliman, 1995). The Gulf of Papua has a broad, low gradient shelf (Walsh et al., 2004). The margin is built up of clinoforms (Walsh et al., 2004; Harris, 1994; Harris et al., 1993, 1996; Slingerland et al., 2008a, 2008b), consisting of topsets, foresets, and bottomsets. The topset is the gently sloped portion located shoreward that rolls over to the steeper dipping foreset at depths of 25–40 m and the bottomset (or pro delta) is the gently sloped portion located basinward of the foreset (Walsh et al., 2004 and references therein). This study uses sediment cores mainly from the bottomset of the Holocene clinothem with depths ranging from 47 to 63 m and two cores from the foreset ranging in depth from 39 to 54 m (Table 1; Fig. 1a).

The Gulf of Papua clinothem is a three-dimensional feature composed of three main lobes: the Southern, Central, and Northern lobes (Fig. 1b; Wei et al., 2018). The three lobes are depocenters of the Holocene clinothem as defined by Holocene sediment thickness and stratal geometry (Slingerland et al., 2008a; Wei et al., 2018). Clinothem geometry observed in the Gulf of Papua records longshore transport as well as infilling of pre-existing morphology. In addition, there are seasonal variations with sediment input during the monsoon and sediment reworking during the tradewind seasons (Walsh et al., 2004; Slingerland et al., 2008b) These processes combine to result in variations in accumulation over short spatial and temporal scales and the possibility of large, event-driven deposits.

A large number of studies have aimed to quantify the sedimentation rates in the area (Harris et al., 1993; Walsh et al., 2004), using sediment traps, ^{210}Pb and radiocarbon. Studies from areas closest to our cores provide evidence for highly variable and sometimes very large sedimentation rates. Walsh et al. (2004) and Harris et al. (1993) show sedimentation rates varying from 0.6 cm/yr up to 5 cm/yr, and show a single large event where sedimentation was as high as 12 cm/yr and lasted 4–5 years. Sedimentation rates vary across the clinothem, as the foreset is the area of fastest sediment accumulation. Additionally, sedimentation rates vary parallel to the margin, with the highest sedimentation rates observed in the Central lobe of the clinothem (Walsh et al., 2004).

3. Materials and methods

3.1. Seismic data and coring sites

Swept-frequency CHIRP seismic data, both from a surface-towed Edgetech system (500 Hz–6 kHz with a 50 ms sweep) and a hull-mounted Knudsen system (3.5 kHz center frequency) (Fig. 1), were

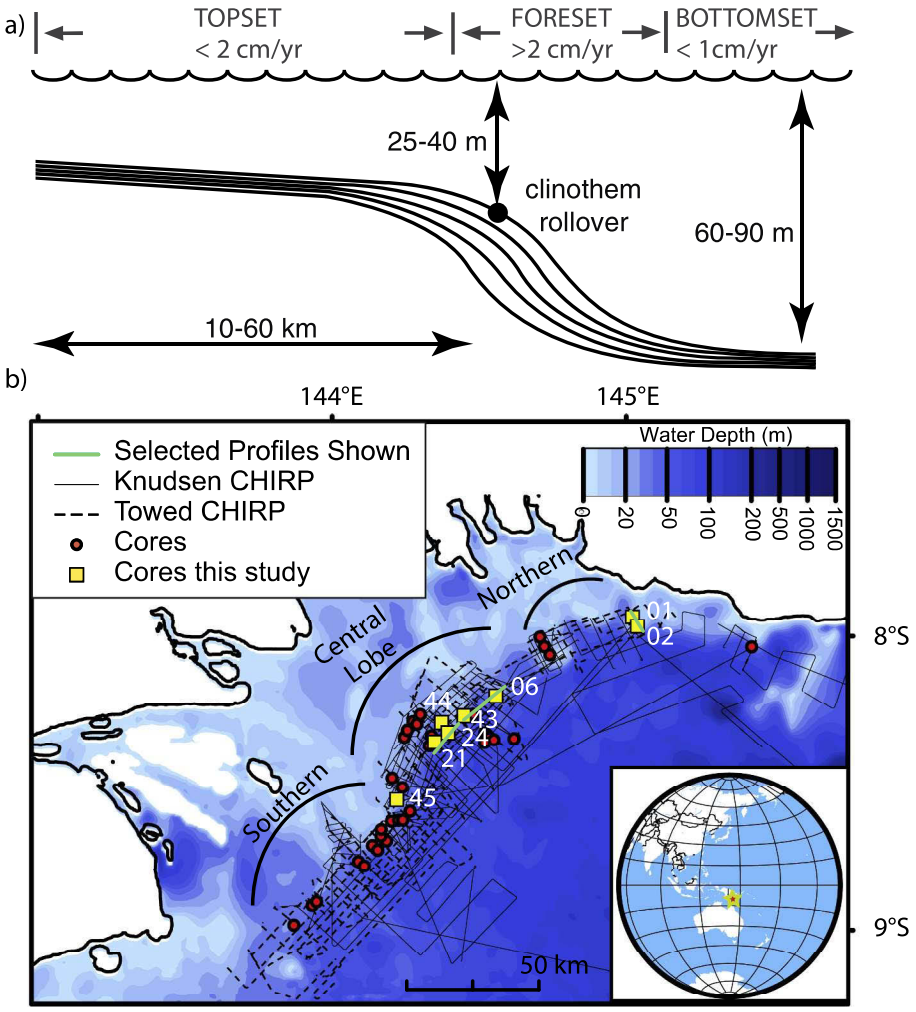

Fig. 1. a) A cartoon of a clinoform showing typical distances, depths and values for sedimentation in the Gulf of Papua based on Walsh et al. (2004). b) A bathymetric map of the GoP showing location of the cores collected (red), cores used in this study (yellow squares), towed CHIRP lines (black dashes), Knudsen CHIRP lines (solid black) and interpreted seismic profiles used in this study (green lines). The inset shows the location of Papua New Guinea. (For interpretation of the references to color in this figure legend, the reader is referred to the web version of this article.)

Table 1
Core locations.

Cores used in this study. Jumbo piston cores (JPC) and companion trigger cores (TC) are listed along with their recovered length, latitude/longitude location, water depth, and a description of their location on the clinoform. The seismic line from cruise VANC22MV that most closely corresponds to each core's location is listed.

Core Name	Length (m)	Latitude	Longitude	Water depth (m)	Location on clinothem	Seismic line
JPC01	8.190	−7.9565	145.03517	53.9	Northern lobe; foreset	mv22-0402-3.5_LF_003
TC01	2.130					
JPC02	9.900	−7.9780	145.04967	62.6	Northern lobe; bottomset	mv22-0402-3.5_LF_008
TC02	1.940					
JPC06	11.13	−8.198	144.57	55.1	Central lobe; bottomset	mv22-0402-3.5a_LF_025 (Line07 in Wei et al., 2018)
TC06	2.030					
JPC21	9.400	−8.37467	144.37317	52.5	Central lobe; bottomset	mv22-0402-3.5a_LF_025 (Line07 in Wei et al., 2018)
TC21	1.97					
JPC24	9.560	−8.33950	144.39183	48.6	Central lobe; bottomset	mv22-0402-3.5a_LF_025 (Line07 in Wei et al., 2018)
TC24	1.830					
JPC43	7.800	−8.28383	144.45817	50.8	Central lobe; bottomset	mv22-0402-3.5a_LF_025 (Line07 in Wei et al., 2018)
TC43	2.060					
JPC44	6.320	−8.30750	144.38117	38.6	Central lobe; foreset	png2L04; png2L05; png2L06
TC44	1.990					
JPC45	6.890	−8.63550	144.23317	47.0	Southern lobe; bottomset	mv22-0402-3.5a_LF_034 (Line03 in Wei et al., 2018)
TC45	2.000					

collected along both strike- and dip-parallel lines between September 2003 and March 2004. They show subsurface layers and reflectors in the sediment 50–100 m below the seafloor with sub-meter resolution (Slingerland et al., 2008a). These were used to identify the stacked clinoforms that make up the margin and to understand the depositional history of the region.

The coring sites and seismic lines from the R/V Melville cruises are shown in Fig. 1b. The cores used in this study are mainly from the bottomset of the clinothem (Table 1) and were chosen to span the length of the margin, which is useful in assessing the internal consistency of the geomagnetic record over tens of kilometers. Most of the cores in this study were collected from the Central lobe of the clinothem, with the exception of jumbo piston cores (JPCs) 01 and 02, which were collected from the Northern lobe, and JPC 45 from the Southern lobe. The tight spacing of seismic data ensures that variations of the clinoform margin can be mapped in the along-shore and downslope directions and additionally ensures that there is detailed contextual information for each collected core. Due to drift during coring operations, some cores were not located precisely on a seismic line but were projected to the nearest line, and in most cases can be reliably projected onto more than a single line.

3.2. Physical analysis and sedimentology

Whole core multi-sensor track (MST) data were collected at Oregon State University prior to splitting the cores. This included P-wave amplitude, resistivity, density, temperature and magnetic susceptibility. Although insufficient calibration information was stored to provide useful estimates of P-wave velocity, resistivity or density, we were able to use the MST to provide reliable magnetic susceptibility data as these data require only a simple volume correction. The cores were later split into halves with a router blade to cut the plastic core liner and a piece of piano wire separated the sediment. One half was kept as a pristine archive half, used for visual core descriptions, and photographs, and the other half was used for sampling for paleomagnetic measurements and radiocarbon dating. The cores were stored in D-tubes and kept refrigerated at the core repository at Scripps Institution of Oceanography. All cores consist mainly of a homogeneous olive grey to dark grey silty clay that sometimes includes very fine, discontinuous sand layers. Cores JPC21 and JPC24 contain a large (30–60 cm) sand layer with a mud matrix and shell fragments that was determined to be an erosional unconformity that represents a transgressive lag deposit formed during sea level rise after the Last Glacial Maximum (Harris et al., 1996; Wei et al., 2018). Sediments below this are thought to have been deposited from 50,000–20,000 years BP (Harris et al., 1996; Slingerland et al., 2008a) and are not a focus of this study.

3.3. Paleomagnetic procedures

The eight cores used in this study visually had many sections of homogeneous, fine- grained material. The jumbo piston cores (JPC) and trigger cores (TC) are 12 cm in diameter and were sampled with a combination of U-channels (inner dimensions 1.8 cm by 2.1 cm) and continuous discrete samples collected in 7 cm^3 plastic cubes (Supplement 1). The cubes were used for measurements of the anisotropy of magnetic susceptibility (AMS) and for directional measurements of all trigger cores as well as JPC21 and JPC45. Samples were taken from the middle of the core to avoid core disturbance near the edges. In a few cases the entire length of the core was not sampled, either due to flow-in at the bottom of the core or because the sediment was too coarse-grained to be sampled.

Anisotropy of magnetic susceptibility (AMS) as well as bulk susceptibility was measured using the Kappabridge KLY-4S and the AMSspin program (Gee et al., 2008). AMS results are described in detail in a future paper. The bulk susceptibility measurements from the Kappabridge show good agreement with the MST whole core susceptibility measurements, for cores where both types of data are available. So for cores where we were unable to collect discrete samples we rely on the MST measurements for susceptibility.

For a small number of representative samples from each core thermomagnetic curves were measured (50 °C/min, 100 mT field, up to 700 °C) to characterize their magnetic mineralogy and material from these samples was measured on the alternating gradient force magnetometer (AGFM) at SIO paleomagnetic laboratory to characterize the domain state. The remanence of discrete samples was measured using a 2G magnetometer at the SIO paleomagnetic laboratory, and U-channel measurements were made at the Institute for Rock Magnetism at University of Minnesota. After measuring the natural remanent magnetization (NRM), the samples were progressively demagnetized using stepwise alternating field demagnetization. This was done at steps of 5, 10, 15, 20, 25, 30, 40, 50 and 70 mT, at which point the sample had reached about 10% of its initial magnetization. The characteristic remanent magnetizations were determined with principal component analysis (Kirschvink, 1980, with the UPMag program of Xuan and Channell, 2009 for analysis of U-channel data) using measurements from all steps 10–70 mT. Samples were also given an anhysteretic remanent magnetization (ARM) in an 80 mT alternating field with a 100 μT bias field. Pilot samples were fully demagnetized to compare the ARM and NRM and demagnetizations. Based on the results of these pilot samples, ARMs of all samples were demagnetized at 5 and 10 mT and this partially demagnetized ARM was used as the normalizer for relative intensity estimates.

To orient different sections of the cores that were not oriented relative to one another during acquisition with a fiducial mark on the liner (for both the piston and trigger cores), we determined the Fisher average of the 10–70 mT PCA directions of the bottommost five points and uppermost five points of each section. The position of the upper most section was held fixed, and the next section was rotated by the average difference in declination between base of the upper section and the top of the next section to ensure that the core declination values aligned at section breaks. This process was repeated until reaching the lowermost core section. The average declination of the trigger core was set to the average declination (5.6°) predicted from the gufm global field model (Jackson et al., 2000) over the past 400 years. Further information on how this was performed is in the supplementary material.

3.4. Radiocarbon dating

Samples of mixed benthic foraminifera were picked from all cores to be used for AMS radiocarbon dating (Table 2). In most cases, a large quantity (about 200 g) of sediment spanning a depth of ~5 cm provided sufficient material (> 2 mg) for dating. Most samples were sent to the Center for Accelerator Mass Spectrometry at Lawrence Livermore National Laboratory; two samples were sent to National Ocean Sciences Accelerator Mass Spectrometry (NOSAMS) facility at Woods Hole Oceanographic Institution. Where possible, a sample was picked from the top and bottom of the trigger core, as well as from the top, middle and bottom of the piston core. This strategy was employed to evaluate whether the trigger and piston cores had recovered the sediment/water interface, and to give a way, independent of magnetic measurements, to determine the offset/overlap between the trigger and piston cores.

This approach was largely successful, with the exception of JPC44, where there was not sufficient dateable material in the bottom of the trigger core, and the sample from the top of the piston core that did not successfully graphitize during the conversion of CO_2 to graphite necessary for radiocarbon dating (T. Guilderson, pers. comm.). This may

Table 2
Radiocarbon ages.
Lab results from AMS dating provided conventional radiocarbon ages (years before 1950) and standard deviation in age for samples. Calibrated radiocarbon ages from Calib 7.1 (Stuiver and Reimer, 1993).

Core	Average sample depth in core (cm)	Conventional radiocarbon age	Standard deviation in age	Calibrated radiocarbon age	1-Sigma	2-Sigma
TC01	9	Modern				
TC01	205	1175	40	715	660–757	626–845
JPC01	38	1220	30	753	686–794	665–873
JPC01	413	1440	30	979	924–1029	885–1108
JPC01	598	1495	40	1036	960–1097	922–1165
JPC01	805	1825	40	1361	1291–1406	1266–1496
TC02	5	> Modern				
TC02	188	860	35	477	441–515	339–556
JPC02	21	1655	35	1207	1165–1265	1079–1265
JPC02	123	2835	35	2580	2507–2677	2408–2717
JPC02	283	2445	30	2075	2000–2135	1941–2244
JPC02	463	6140	30	6561	6498–6623	6431–6675
JPC02	943	9480	100	10,333	10,206–10,445	10,107–10,598
TC06	10	> Modern				
TC06	198	785	30	414	365–474	305–492
JPC06	13	830	30	455	421–498	333–522
JPC06	253	1460	80	1005	909–1103	803–1203
JPC06	523	1710	30	1257	1212–1301	1162–1348
JPC06	1073	2015	40	1570	1506–1647	1414–1703
TC21	8	> Modern				
TC21	188	630	30	265	148–317	129–396
JPC21	7	585	25	204	145–268	68–301
JPC21	69	4185	30	4259	4180–4340	4115–4401
JPC21	90	5165	30	5518	5474–5569	5410–5625
TC24	15	> Modern				
TC24	176	500	30	112	0–173	0–234
JPC24	7	390	30	Post ad 1950		
JPC24	243	950	35	544	499–595	475–631
JPC24	390	3880	30	3835	3760–3907	3688–3968
TC43	7	> Modern				
TC43	198	645	30	283	237–359	142–405
JPC43	13	995	30	576	535–616	504–646
JPC43	373	1820	30	1353	1294–1394	1267–1478
JPC43	548	2400	90	2027	1894–2138	1810–2288
JPC43	723	2070	35	1633	1561–1691	1514–1774
JPC44	26	710	35	351	293–401	261–453
JPC44	163	900	35	506	467–539	430–608
JPC44	313	775	30	404	337–462	301–486
TC45	163	> Modern				
JPC45	53	555	30	175	124–256	0–279
JPC45	103	370	70	Post ad 1950		
JPC45	153	620	35	251	147–303	106–396
JPC45	203	640	30	277	230–359	138–402
JPC45	253	600	30	222	146–282	65–330
JPC45	303	565	30	184	133–258	0–287
JPC45	353	640	30	277	230–359	138–402
JPC45	403	640	30	277	230–359	138–402
JPC45	453	675	30	318	265–372	151–444
JPC45	503	665	35	306	256–372	146–430
JPC45	553	645	25	283	237–356	145–401
JPC45	603	600	30	222	146–282	65–330
JPC45	653	620	35	251	147–303	106–396

have been caused by sulfur in the sample, which would likely indicate a reducing environment. Unfortunately, we could not obtain another sample to determine the source of the problem, and as a result JPC44 has poor age constraints.

We initially collected 13 samples of foraminifera at 50 cm spacing from JPC45 to be dated and to ensure we had at least one well-dated core. The calibrated radiocarbon ages for this core, however, had a narrow range from modern to 351 years BP. Two additional samples, from 355 and 605 cm were picked and sent to NOSAMS to rule out the possibility of lab error. The ages came back identical to those previously determined. The conventional radiocarbon ages were calibrated using Calib 7.1 (Stuiver and Reimer, 1993) and the Marine13 (Reimer et al., 2013) curve with an estimated Delta R of 10. Although using the CHRONO marine reservoir database and selecting many nearby records will not give this estimate of reservoir age (the seven closest records will give an estimate of Delta R = −3, Gillespie and Polach, 1979, McGregor et al., 2008, Rhodes et al., 1980, Chappell and Polach, 1976) we determined that the highest quality and most representative data to use for determining Delta R came from Burr et al. (2009) which used precisely dated corals from the South Pacific ~950 km away. Previous

radiocarbon ages collected from the Gulf of Papua cores (Harris et al., 1996; Johnstone, 2012) sampled material other than forams (peat, ooids, mollusk shells, bulk carbonate for example) and obtained anomalously old ages compared to our results, as well as dates out of stratigraphic order. Some of this material was likely reworked and these earlier radiocarbon ages are not used for establishing our age scale.

4. Results

4.1. Alignment of the piston and trigger cores

In ideal circumstances, the piston coring system has a trigger core that is designed to capture the uppermost sediment and duplicate the upper few meters of sediment captured by the piston core. The trigger core is a short (~2 m) weighted gravity core that is suspended adjacent to the piston core, at some length (approximately 20 ft) below it. The impact of the trigger core with the seafloor releases the piston core, and a length of wire will ideally stop the piston at the seafloor, while the piston core barrel penetrates beyond the piston. However, there are many problems associated with this process of piston coring. The problems are common but complex (Lunne and Long, 2006 provide a review of seabed samplers that discusses many of these problems) and can include over penetration of the piston core, potentially caused by poor placement of the piston or incorrect estimates for the length of slack wire (Buckley et al., 1994) or rebound of the wire due to releasing the piston core. The amount of over penetration may be significant and some paleomagnetic studies (Lisé-Pronovost et al., 2009, Barletta et al., 2008, Peck et al., 1996) have estimated the over penetration by comparing the susceptibilities of piston core top to the trigger core and finding the best fit. These studies reveal that over penetration of up to 400 cm may occur (Peck et al., 1996). Here we employ a similar strategy but, before comparing magnetic susceptibilities, we use ^{14}C dates from the trigger core bottom and piston core top to restrict the possible offset, only allowing the range of possible offsets to fit within the one sigma error of the radiocarbon dates, assuming a linear sedimentation rate. We determine the best fit of the magnetic susceptibilities using the root mean square error after linear interpolation between measured points. Because the tops of trigger cores had recent ages, data from the piston core is moved in 1 cm increments relative to the trigger core, within the range of predicted offsets and we determined the offset by minimizing the misfit of the susceptibility profiles. For cores where there was no overlap, the offset was determined using the linear sedimentation rate of the trigger core as it has less potential deformation.

After determining the offset for the piston core, the average declination of the trigger core was set to the present-day declination at the site (5.6°) and a rotation was applied to the entire piston core so that the averages of overlapping points agreed. For cases where there was no overlap, the average declination of the top 50 cm of the piston core was aligned to the bottom 50 cm of the trigger core. There was a single core (JPC44) where we could not obtain an age from the bottom of the trigger core. To determine the offset of this core, we used the following methods. The magnetic susceptibility of the trigger and piston cores differ by almost a factor of two, so there is likely no overlap. If the two dates from within JPC44 represent a constant sedimentation rate (5.4 cm/yr), and we employ this sedimentation rate to calculate the offset distance from a recent age at the top of the trigger core, the calculated offset of the piston core would be 16.7 m. This unrealistic offset, however, is subject to uncertainties because sedimentation rates calculated from two dates with a short time span between them (at the tops of cores where both dates are recent, for example) are oftentimes higher than rates calculated from dates with a long time span between them (using an older date from the middle of the core along with a recent date, for example) (Sadler, 1981). A minimum possible offset of 200 cm is assumed, which is reasonable considering the offsets found in other cores (range from 0 to 268 cm for seven of the cores, and 426 cm for a single core). Refinement of the offset depth for JPC44 would affect how the trigger core and upper 226 cm of the piston core are mapped to age, but the effect of these changes will be minimized when stacked due to the number of cores that have data in the 0–350 year range.

The radiocarbon age collected from the top of JPC24 piston core was the only piston core age (aside from a single age in JPC45) that had a modern age. Using this information, the offset of the piston core was assumed to be 0 cm, meaning the upper 200 cm captured the same time period as the companion trigger core. The declinations of these two do not appear compatible with each other, as they trend in opposite directions, but there is not sufficient evidence from either set of measurements to regard one as more reliable than the other.

The calculated offsets ranged from 426 cm (JPC02) to no offset (JPC24) and are shown with the susceptibilities (Fig. 2) to illustrate the goodness of fit for the reader. In the figure, the susceptibility values collected from discrete cubes (acquired assuming a nominal 10 cm^3 volume) and are left uncorrected for the true volume to allow a slight offset between the MST data and cube data. The volume-corrected bulk susceptibility data for the 7 cm^3 discrete samples brings the two sets of susceptibility data to nearly identical values.

4.2. Remanence directions

The remanence directions are all nearly univectorial, with a small overprint that is typically removed by 10 mT (Fig. 3). The median destructive field (MDF, the alternating field (AF) value at which the remanence is reduced by half) values show little variation, and 95% are between 21 and 30 mT. Cores that were measured using discrete cubes (all trigger cores and the JPC45 and JPC21 piston cores) were demagnetized using $+X, +Y, +Z$ and $-X, -Y, -Z$ on alternating steps to allow identification of any spurious remanence due to a non-zero field in demagnetizer. Remanence directions from these alternate steps generally show no detectable difference in direction. A small number of samples have less ideal demagnetization behavior. For example, JPC21 (Fig. 3c) represents a coarse-grained sample from the transgressive surface. These coarse-grained samples were excluded from our study. Generally, the maximum angular deviation (MAD) of the principal eigenvector values were very low ($< 3°$) although some points near section breaks or in portions of the less consolidated trigger cores exhibited higher MAD values, though still $< 5°$. For U-channel samples, the response functions of the magnetometer coils result in smoothing of the data and edge effects at the ends of sections (Jackson et al., 2010). Measurements within approximately 5 cm of each section end were not used due to these edge effects. In a few cases (mainly the transgressive surfaces found in cores JPC21 and JPC24, and the base of JPC02) the MAD values were very high ($> 15°$).

4.3. Magnetic mineralogy and suitability for paleointensity

The use of sediments for relative paleointensity determinations relies on the assumption that the remanence acquired is proportional to the field value and that variations in con- centration of the magnetic minerals can be adequately accounted for by the normalization. Criteria aimed at establishing this are 1) the magnetization should be carried by magnetite in the 1–15 μm single domain/pseudo-single domain (SD/PSD) range (King et al., 1983), 2) the concentration of magnetite should not vary down core by more than a factor of 10 (Tauxe, 1993) the NRM should be defined by a single component of magnetization with

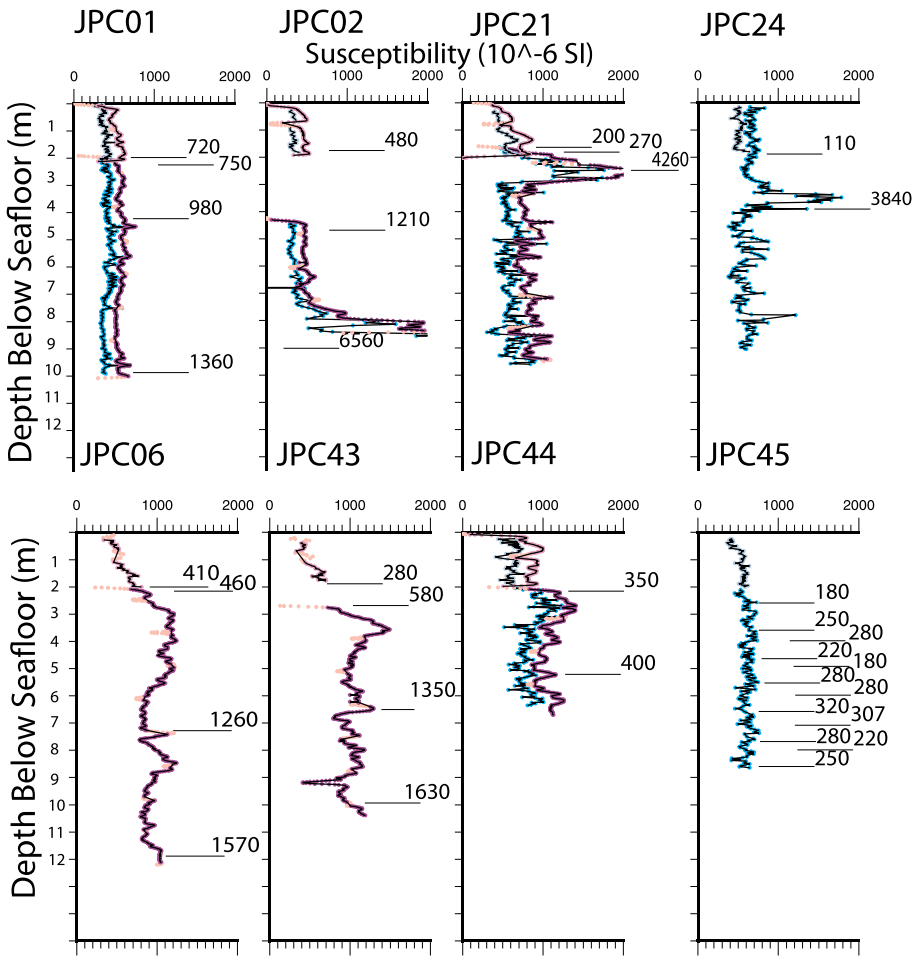

Fig. 2. Magnetic susceptibility for all cores used in this study plotted against depth below seafloor. Susceptibility data collected using cubes is shown in light blue (cyan) for the trigger core (piston core). Multi-sensor track susceptibility data is shown in deep pink (purple) for the trigger core (piston core), with light pink to show data from the ends of sections. Black lines indicate depths where samples were collected for radiocarbon dating (including the piston core offset), and the calibrated radiocarbon age in years BP rounded to the nearest decade is noted. (For interpretation of the references to color in this figure legend, the reader is referred to the web version of this article.)

MAD < 5° (Stoner and St-Onge, 2007), and 4) the normalizer should have a similar demagnetization curve to that of the NRM (Levi and Banerjee, 1976).

Thermomagnetic curves (Fig. 4) in all cases reveal a discernible Curie point on the heating curves (575 °C) that is compatible with the presence of low-Ti titanomagnetite. The curves range from nearly reversible with a single high Curie point to curves with more distributed Curie temperatures, suggestive of a range of magnetic minerals, and significant increases on cooling. The irreversibility of most curves, together with an increase in magnetization above 500 °C on some heating curves, suggests that additional magnetite is formed during heating. Notably, none of the curves display a significant magnetization decrease over the interval (280–430 °C) expected for the breakdown of griegite (e.g., Bol'shakov and Dolotov, 2012; Ron et al., 2007; Brachfeld et al., 2009). We suggest that the thermomagnetic data are most compatible with a range of titanomagnetite compositions, including low-Ti titanomagnetite, which should be suitable for relative intensity determinations. The volcanic source rocks (Slingerland et al., 2008a) supplying material to the Gulf of Papua are consistent with this interpretation of a range of titanomagnetite compositions.

The shape of the hysteresis curves is characteristic of the pseudo-single domain region on a Day plot and most samples plot in the PSD region (Day et al., 1977) that should be suitable for relative intensity studies. Despite the color of the sediments, which might suggest the possible presence of greigite, the hysteresis parameters for measured samples also do not indicate the presence of greigite (Mrs/Ms ≈ 0.5 and Bcr/Bc ≈ 1.5, Roberts, 1995), nor do the heating curves, but these were not measured exhaustively. Other studies have shown that greigite may be identified by an increase in the median destructive field of the NRM (Brachfeld et al., 2009) or by an acquisition of a gyromagnetic remanent magnetization (GRM) exhibited as an intensity increase and acquisition along the last axis of demagnetization (e.g. Snowball, 1997; Frank et al., 2007). Neither of these features were noted in our cores from the Gulf of Papua and so we conclude that variable amounts of PSD (titano)magnetite carry the remanence in these cores.

The concentration variations of pseudo-single domain (titano) magnetite in the Gulf of Papua cores also appears to be well within the range accepted for determining sedimentary relative intensity, shown by the minimal variations in susceptibility (Fig. 5). Following King et al. (1983) we have plotted anhysteretic susceptibility (ARM, the anhysteretic magnetization acquired per unit bias field, Tauxe, 1993) versus low-field susceptibility (K) and compared it with the simple phenomenological model of King et al. (1983) as a measure of magnetite grain size and concentration. ARM is more sensitive to single domain and pseudo-single domain grains, whereas K will be more sensitive to large pseudo single domain or multi-domain grains and the ratio of the two can thus be used to give an estimate of relative particle size. The comparison to the phenomenological model based on sized magnetite

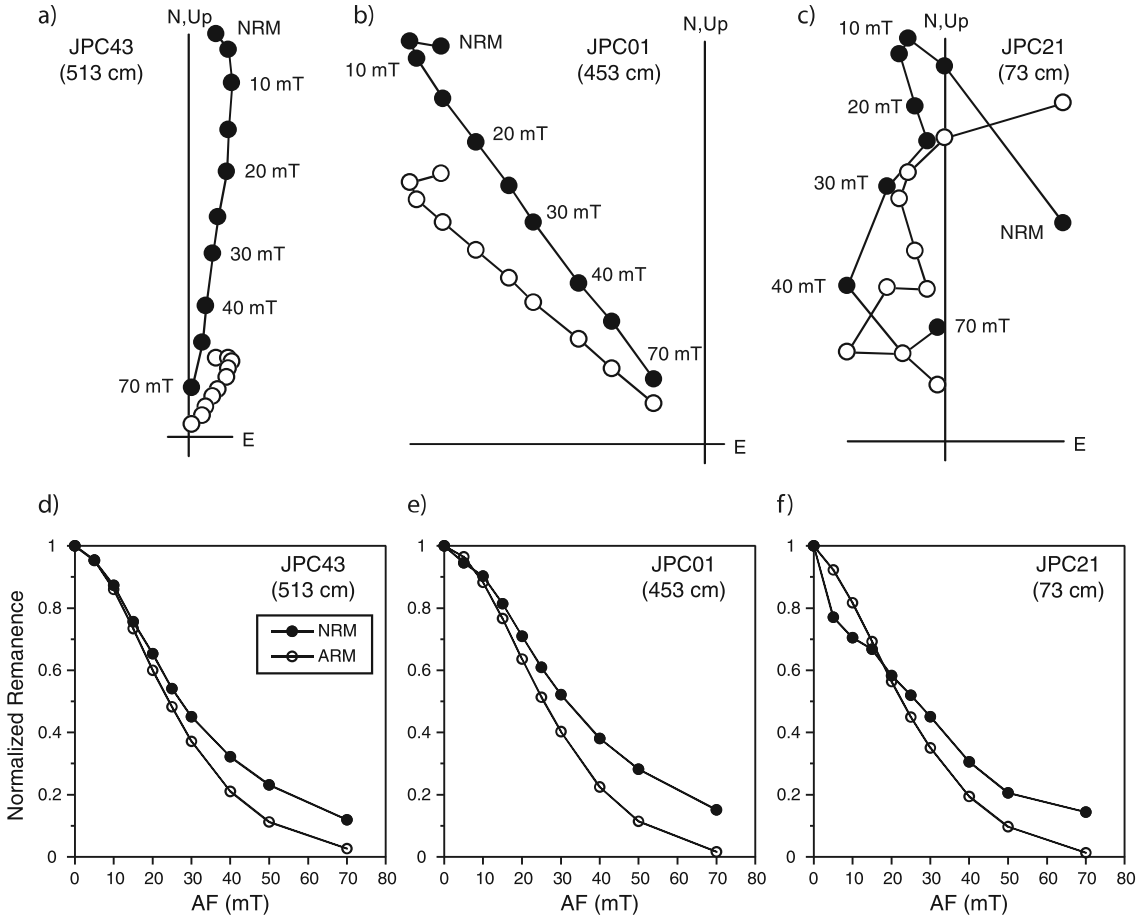

Fig. 3. Representative vector end-point orthogonal projections for typical samples (a, b) and a sample from the coarse-grained transgressive surface (c). Corresponding normalized demagnetization curves are shown in d, e, f.

data (King et al., 1982) provides an estimate of magnetite grain size and all cores fall generally below the upper 15 μm range limit. Individual cores plot in a cluster (Fig. 5), indicating a consistent grain size. JPC24 has two distinct grain size and concentration clusters, and these correspond to the samples from above (lower cluster) and below (upper cluster) the transgressive surface.

The consistent grain sizes, minimal changes in susceptibility, and single component NRM with low MAD values satisfy the criteria outlined for suitable paleointensity studies. The overall similarity of the demagnetization curves of NRM and ARM (Fig. 3) illustrate the suitability of ARM as a normalizer, and the relative paleointensity, calculated using NRM intensity at 10 divided by ARM intensity at 10 mT and the normalized to the mean, is shown in Fig. 6. Additional information showing suitability of NRM_{10mT}/ARM_{10mT} as an RPI proxy can be found in the supplementary material.

Fig. 6 shows relative declination, inclination and relative paleointensity (NRM_{10mT}/ARM_{10mT} normalized to the mean) as a function of depth below seafloor. It is evident from this figure that the cores are very homogeneous, with few features to note on the lithological section, and mainly small variations in susceptibility, except for some very large increases related to the transgressive lag deposit in JPC02, JPC21 and JPC24. The MAD values are very small and there is little variation in the MDF values. There are similar inclination values in most cores, near −20° and shallower than the present day inclination at the site (~ −30° from the IGRF). The declination values in the piston cores are less consistent and seem to exhibit signs of twisting (JPC01 and JPC44 for example), but the declination values in trigger cores show eastward trends. The transgressive lag deposit is evident in JPC21 and JPC24 and is accompanied by a large change in inclination. This large inclination is not evident in JPC02 and this is likely age related — at a depth of 9.46 m in JPC 02, the age is ~10,000 BP, while the age of the sediment below this surface in JPC 21 and JPC24 is much older. It is apparent in some cores, JPC06 and JPC44 for example, that the inclination is discontinuous across section boundaries, indicating some physical deformation that likely occurred during the sectioning process. Further explanation about the physical deformation at section boundaries and how measurements near the boundaries were taken into account is explained in the supplementary material.

4.4. Seismic correlation

One of the goals motivating this study was to determine whether the abundant seismic data from the Gulf of Papua margin could provide complementary information to radiocarbon ages in establishing the correlations between cores. The seismic data allow recognition of four distinct sedimentary sequences described by Slingerland et al. (2008a, 2008b) and Wei et al. (2018; Fig. 7). At the base of the section is an older clinothem that has been incised and eroded (Unit C; shown in

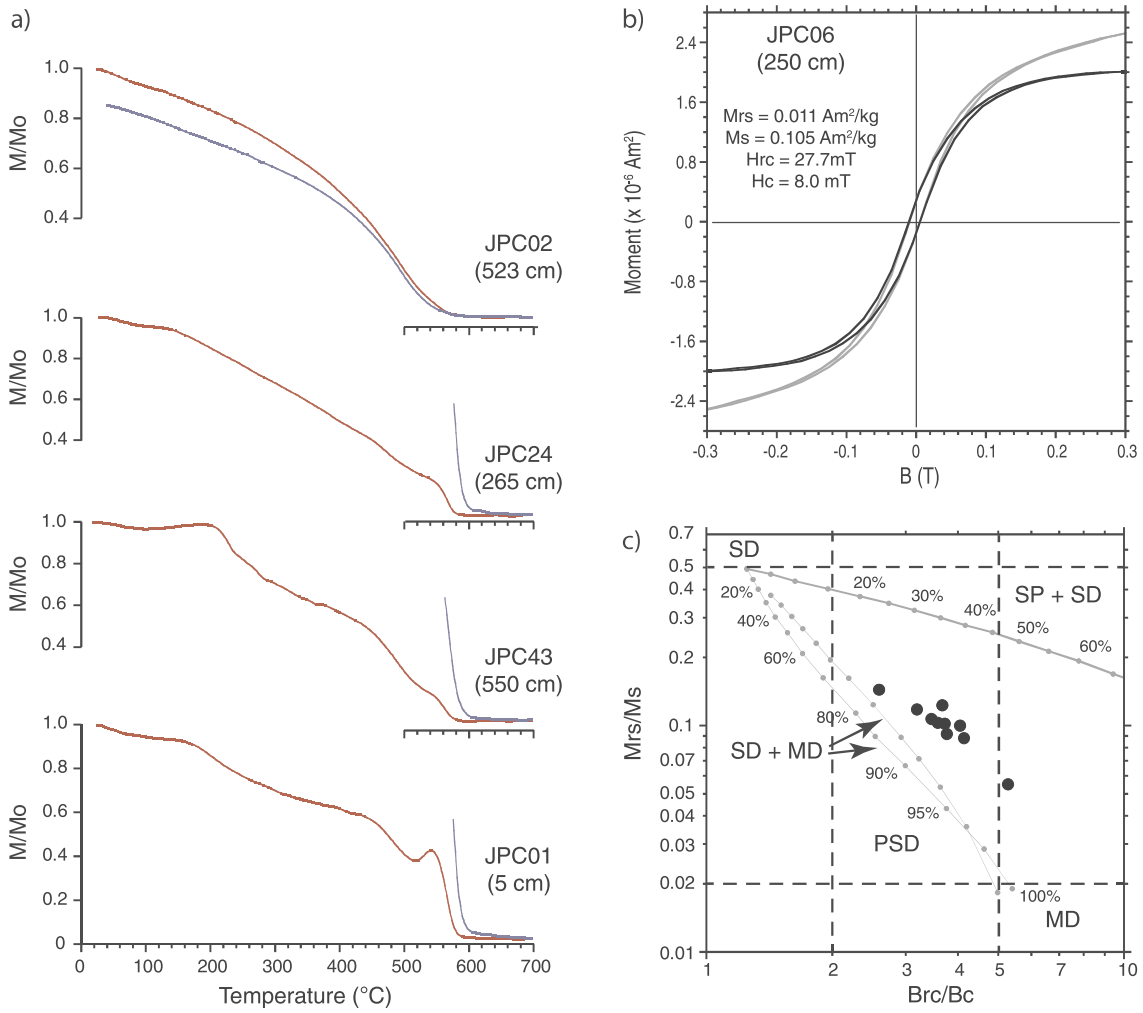

Fig. 4. a) Representative heating (red) and cooling (blue) curves. b) Typical hysteresis curve and derived parameters. The coercivity of magnetic minerals (Hc), the coercivity of remanence (Hcr) the saturation remanence (Mrs), and the saturation magnetization (Ms) are indicated. c) Day plot (Day 1977) of samples from all eight cores. Most fall in the pseudo-single domain (PSD) region. (For interpretation of the references to color in this figure legend, the reader is referred to the web version of this article.)

blue), mantled by a transgressive deposit (Unit B1; shown in green). The Holocene clinothem progrades out across this surface with the Yellow package (Unit A1) being more progradational and the Orange package (Unit A2) having more aggradational geometry than Yellow. Separating the Yellow and overlying Orange package is a surface of lap, called S1 (Slingerland et al., 2008a, 2008b). Above Orange is an aggradational Red unit (A3) that is characterized by two reflectors (pink and purple) that can be observed in all lobes of the clinoform. The boundary between Orange and the most recent Red package is another surface of lap, called S2 (Slingerland et al., 2008a, 2008b). Distinctive reflectors within the Orange and Red seismic packages were traced, whenever possible, between the locations of the cores. A seismic reflector is an impedance contrast and in the Gulf of Papua it could represent an event, such as an erosional surface or changes in the sediment characteristics (e.g., a deposit during trade winds season). After picking two-way travel times for the reflectors, we converted these travel times to depth below seafloor using a velocity of 1300 m/s. Although this is low compared to literature values that commonly use a two-way travel time velocity of 1500 m/s, lower values for seismic velocity have been used successfully in Fallen Leaf Lake matching reflector depths to identifiable features in cores (Maloney et al., 2013), and east of the MacKenzie River, where P wave velocity of the core logged at sea was 1333 m/s (Keigwin et al., 2018).

Additionally, the 4.26 m offset determined from radiocarbon ages for JPC02 is consistent with the location of the transgressive surface identified in the seismic data (Fig. 8). With this 4.26 m offset, the top of the erosional surface (shown as shaded region of the core), which was identified in the core by ooids and coarse sediment, approximately coincides with the high amplitude reflector that we recognize as a regional erosional surface.

Fig. 7 shows an uninterpreted and interpreted seismic profile (the location of the line shown is highlighted in Fig. 1) and the locations of two cores (JPC06 and JPC43) on this strike-parallel seismic line. The two cores are located about 10 km apart, and the majority of the reflectors can be traced laterally between the core sites (Fig. 7). The radiocarbon ages obtained from each core (Table 2) indicate similar sedimentation rates at the two coring sites. The compatibility of the seismic reflectors with the radiocarbon ages (bottom panel Fig. 7)

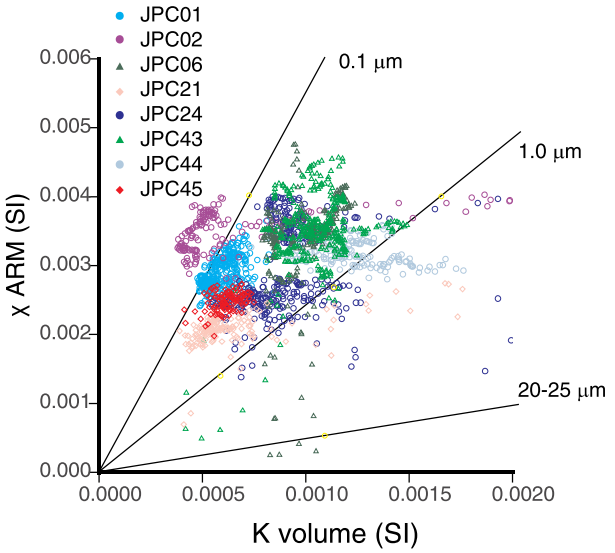

Fig. 5. Anhysteretic susceptibility (χARM) versus volume normalized low field susceptibility (K) after King et al. (1982) to show relative grain size variations in magnetite. Idealized model from King et al. (1983) is shown with black lines. Circles indicate χARM from U-channels and K from cubes measured, Triangles indicate χARM from U-channels and K from multi-sensor track, diamonds indicate χARM and K from cubes. K from cubes is normalized to the correct 7 cm^3 volume.

indicates that these two cores likely have similar depositional history.

Although the overall consistency of the apparent ages of reflectors between cores JPC06 and JPC43 is encouraging (Fig. 7), the large distances between cores and differences in sediment source along the margin make using seismic reflectors as temporal markers between lobes impossible. The reflectors within these sequences were identified based on acoustic character and stratal relationships. It is difficult to trace these reflectors between the lobes due to pinchout and truncation due to toplap, but within a lobe our preferred interpretation is that the reflectors have time significance. However, these reflectors are not identifiable everywhere. For example, high accumulation rate cores JPC44 and JCP45 nominally correspond with the Red seismic package but lack the Pink and Purple reflectors characteristic of this unit elsewhere. JPC 45 is located in the southern lobe and in a broad topographic low defined by the topography of the underlying blue sequence. It is possible that the high accumulation rates in this location are due to gravity flows. Reflectors were not continuously traced between lobes but nonetheless it is plausible that the changes in geometry may have a general time significance. The systematic increase in age with depth shown in Fig. 9 generally supports such a relationship and is encouraging from a paleomagnetic perspective, because it suggests that the sedimentation was continuous, with few large gaps in the data.

4.5. Age model

Radiocarbon ages document significant variation in sediment accumulation rates (Fig. 10) and the eight cores display various degrees of continuity (Fig. 7), due to both piston core offsets and hiatuses in the record. JPC01, JPC06, and JPC43 appear to span approximately 1500 years with relatively continuous sedimentation. All the trigger cores also appear to represent continuous sedimentation, but the trigger cores for JPC01 and JPC02 appear to have a much lower sedimentation rate than cores farther southwest in the Gulf of Papua.

JPC44 and JPC45 are two cores that have extremely high sedimentation rates. Two dates within JPC44 gave a sedimentation rate of 5.4 cm/year. In JPC45, 680 cm of sediment accumulated in the last 350 years BP. These variable and sometimes extremely large sedimentation rates are not a surprise (see Walsh et al., 2004 and Harris et al., 1993), but they can be used to make a strong case for converting measurements from depth to age using a core's own chronology.

The only hiatus that can be confidently identified is that associated with the transgressive surface; there is no visual evidence of other discrete events though they could be present. JPC02 extends back about 2000 years before encountering this hiatus, below which ages are significantly older (> 6000 years BP). JPC21 and JPC24 have high sedimentation rates in the sections above the transgressive surface, but below the surface there were insufficient benthic foraminifera to perform radiocarbon dating. Samples from within the transgressive deposit were dated and yield ages > 3500 years BP that may be used for estimating timing of the deposit, but this is not the focus of this study. The ages predating the transgressive deposit from JPC02, JPC21 and JPC24 (Table 2) are not plotted or used in establishing an age-depth model because they span a hiatus or are obtained from potentially reworked material overlying an erosional unconformity.

While some studies do not use radiocarbon ages directly, but instead transfer age information from one core to another using correlations based on susceptibility or remanence, in this complex depositional setting that method is not appropriate. All cores are converted to age using a linear regression to find a best fitting line that passes through the origin, because the tops of all cores gave greater than modern radiocarbon ages. We do this for all cores, except JPC06 which is best represented by two straight line segments fit to the radiocarbon ages.

4.6. Stacking

Although the cores measured in this study collectively cover a time back to 2000 years BP, few cores cover that span continuously (Fig. 11). The most recent 300 years are recorded in every core as all cores have present-day radiocarbon ages at the tops of the trigger cores. JPC01, JPC06 and JPC43 provide records back to approximately 1600 years, and JPC02 extends back approximately 2000 years; however, it is missing approximately 600 years of time between the trigger and piston cores due to the over penetration of the piston core. JPC44 and JPC45 cover the most recent 300 years with extremely high resolution, but provide minimal coverage before then. All trigger cores exhibit a consistent declination change, showing an easterly drift from approximately 500 years BP to present. However, piston cores that cover that same interval do not necessarily replicate that change. Of particular note is JPC24, where the piston core and trigger core appear to overlap completely in time but do not show the same trend in declination. JPC44 also shows an opposite trend in declination between the piston core and trigger core. Most of the cores have inclinations that get less steep, and closer to the geocentric axial dipole (GAD) value expected at the site, deeper in the core, although JPC24 is an exception, with inclinations in the trigger core lying close to the GAD value.

The high accumulation rates of JPC44 and JPC45 mean that the resolution of the first 300 years is better compared to the resolution in cores with lower sedimentation rates over the last 300 years. The differences in accumulation rates change our approach to stacking. While previous studies (e.g., Constable and McElhinny, 1985) interpolate a single value of inclination, declination and relative paleointensity to evenly spaced depths for each core, this approach would not translate well to this study. For example, a single interpolation scheme based on the lower resolution cores would eliminate data from the higher resolution ones. Conversely, an interpolation based on the higher

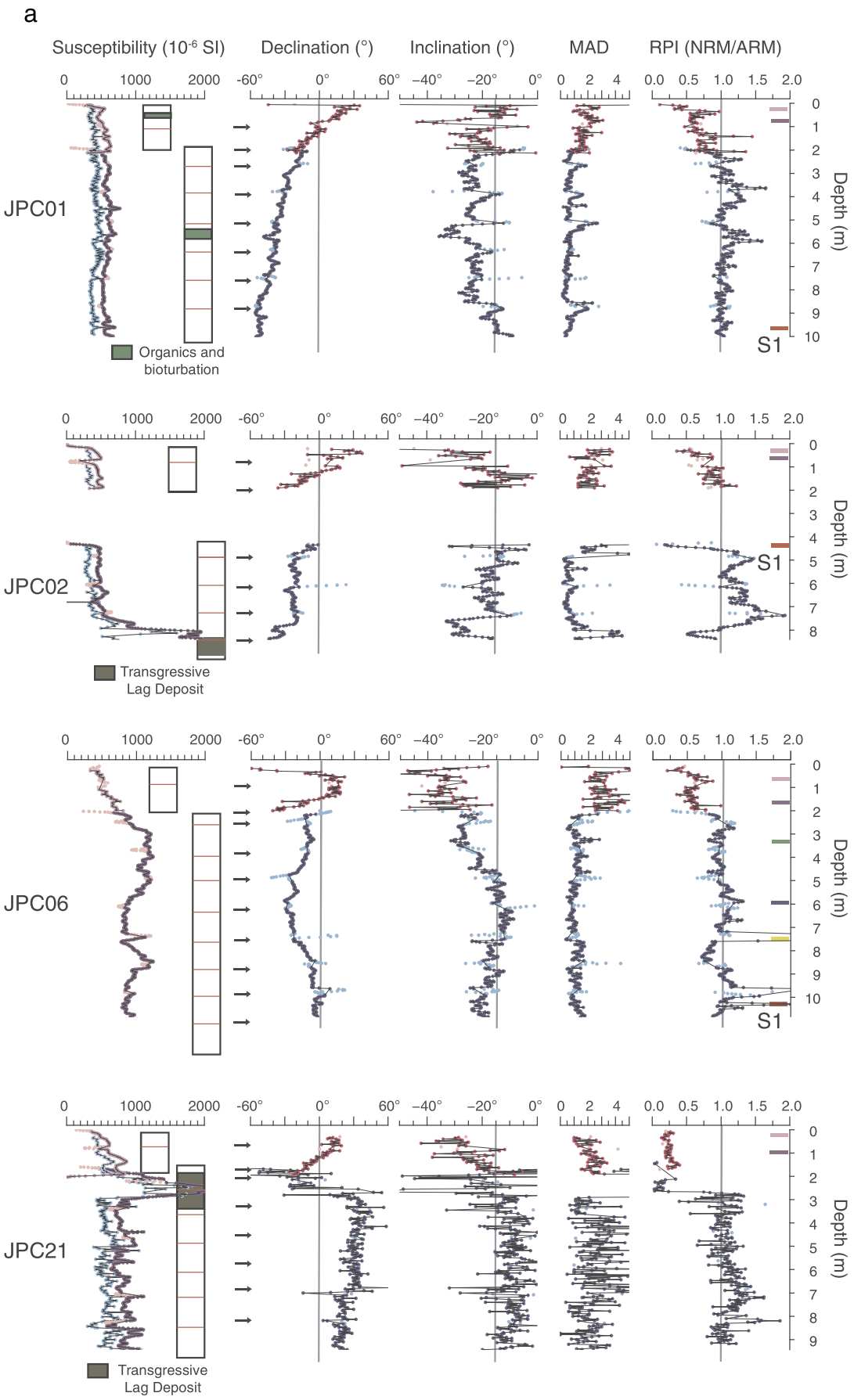

(caption on next page)

Fig. 6. Magnetic susceptibility and directional data for all cores used in this study plotted against depth below seafloor, with piston core offsets included. Susceptibility data collected using cubes is shown in light blue (cyan) for the trigger core (piston core). Multi-sensor track susceptibility data is shown in deep pink (purple) for the trigger core (piston core), with light pink to show data from the ends of sections. Representations of the visual core descriptions are depicted with the trigger core and piston core offset and red lines and arrows indicating the section boundaries. Cores that appear blank had no visual features of note. Relative declination, inclination, maximum angle of deviation (MAD) and relative paleointensity (RPI) are plotted in deep pink (blue) for the trigger (piston) core. Light pink (cyan) represents points from the ends of trigger (piston) core sections that were not used due to disturbance and/or response function of the magnetometer. The expected dipole inclination at the site is shown with a grey line. Colored bars at the far right indicate seismic reflector depths and correspond to Fig. 7. (For interpretation of the references to color in this figure legend, the reader is referred to the web version of this article.)

sedimentation rate cores would result in a substantial fraction of interpolated data in the more slowly accumulated cores. We take a Fisher average of the inclination and declination data after binning into 20 year non-overlapping intervals, as a compromise between the low and high sedimentation rate cores, and calculate an alpha 95 confidence interval. A small amount of data was not included in the stack – the section of JPC44 that had a nearly instantaneous 100° shift in declination was removed prior to binning and averaging data.

To plot relative paleointensity versus depth in Fig. 6, the values of NRM_{10mT}/ARM_{10mT} were divided by the mean of the entire core. The result of this in JPC21 and JPC24 is a very low relative paleointensity in the section above the transgressive surface and a larger value for the sections below the surface. The only conclusions that can be drawn from this are that the intensity of the field in the last 300 years is lower than the intensity of the field at some prior, unknown time. Therefore, in Fig. 11, the values for JPC21 and JPC24 have been divided by the mean of the only the data from above the transgressive surface in these cores.

5. Discussion

The Gulf of Papua cores collectively provide a high-accumulation rate record of geomagnetic field from 2000 to present, helping to fill a major gap in the current global sedimentary field data. High resolution studies like this one are essential for refining our current Holocene field models. In this study, the broad inclination record is probably the most robust feature of the data, and an apparent trend for the past 2000 years observed in Fig. 12 is a steepening in inclination from −20° to the present-day value at the site of −30°. The declination has an eastward trend since 1400 years BP, and the relative paleointensity has been decreasing. Although data from the past 2000 years are shown, 1600–2000 years BP should be treated with caution, as it represents only one or two cores from the region. The abrupt change in inclination, declination, and paleointensity near 1600 years is due to the lower portion of the stack being calculated from only a single core and is not robust.

There are few complete, high-resolution records for 0–2000 years in this region. In addition to comparing our results to ODP Hole 1202B (4360 km away, Richter et al., 2006), and Lake Pounui (4780 km away, Turner and Lillis, 1994), we plot predictions at this site from the CALS3k.4 (Korte and Constable, 2011) and pfm9k (Nilsson et al., 2014) field models. The Holocene sedimentary paleofield record closest to the Gulf of Papua is the record from Lake Kailampaa (Haberzettl et al., 2013). The age model from this record is difficult to evaluate since all the dates were on bulk sediment and repeat analyses from multiple labs gave discrepant results. Given this poorly constrained age model, we have made no comparisons to this nearby record. Our record and the ODP Hole 1202B show a decrease in paleointensity over the last 2000 years (Fig. 12). The long-term trends of these two records is remarkably similar and potentially even smaller-scale features may correlate – see for example 1800–1300 years BP or 600–200 years BP. The Lake Pounui record of declination shows a similar long-term trend to this study with a steady eastward trending portion from 1600 years BP to present.

Both inclination records exhibit the same pattern of steepening inclination. Generally, the records shown here exhibit better agreement amongst themselves than with predictions from the models. For example, the inclination of the models exhibits a shallowing from 1440 to present day compared to the two records, and the relative intensity of the models shows very little variation compared to the records shown. The addition of more sediment directional and paleointensity data as well as archeomagnetic data should help to refine the models in these areas.

Although early studies had concluded that westward drift was the dominant movement of non-dipolar parts of the field (e.g., Bullard et al., 1950; Vestine, 1953; Nagata, 1965), further studies showed more complex motions of the non-dipolar part of the field, including episodes of eastward drift. Westward drift was initially explained by Bullard et al. (1950) using dynamo theory that required the outer part of the core to rotate less rapidly than the inner part. This uniform view of the magnetic field coupled the solid mantle to the core as a whole, and features of the field moved westward with the motion of the outer part of the core Analysis of the global field model CALS7k.2 (Korte and Constable, 2005) by Wardinski and Korte (2008) and Dumberry and Finlay (2007) showed both eastward and westward drift. While westward drift of high latitude flux patches and features in the Atlantic appear to be real (Nilsson et al., 2014), confirmation of westward drift in the southern hemisphere is limited due to the lack of data and limited resolution of the models in that region. The trend in declination from our new record does not suggest westward drift in this time period.

As noted previously, there are a number of different techniques that can be used to establish tie points between cores. The most suitable features to use as tie points should have a well-known date and be continuous over the region of study, which usually requires a good understanding of the process or mechanism by which that feature is generated. There are examples of this, such as susceptibility changes related to glacial/interglacial variations, where the origin of the variations has a satisfying physical explanation (e.g., Lean and McCave, 1998; Sakai et al., 2000). Nevertheless, poor theoretical understanding of how sediments record the geomagnetic field should discourage one from attempting to match multiple inclination and declination features that appear on very short time scales or over large distances.

Susceptibility can be useful for establishing tie points, but it also can suffer from the same problems as matching inclination and declination changes in susceptibility and are not unique to specific causes or processes. It could be related to a time transgressive deposit, as was seen in this study, or it could be due to natural variation in sedimentation that is not necessarily continuous across the spatial scale of the study. In both cases of susceptibility and inclination/declination matching, matches should be made only if there is some level of coherence at the scale of interest. In our study we chose to combine cores based on their own chronology based on radiocarbon data and are consistent with stratigraphic correlation, because the complexities in the environment were simply too great to assume that variations in susceptibility had a relevant time association.

One of the more puzzling aspects of the Papua New Guinea records is the presence of apparent rapid (approximately instantaneous) changes in the declination within a core section. Several cores had

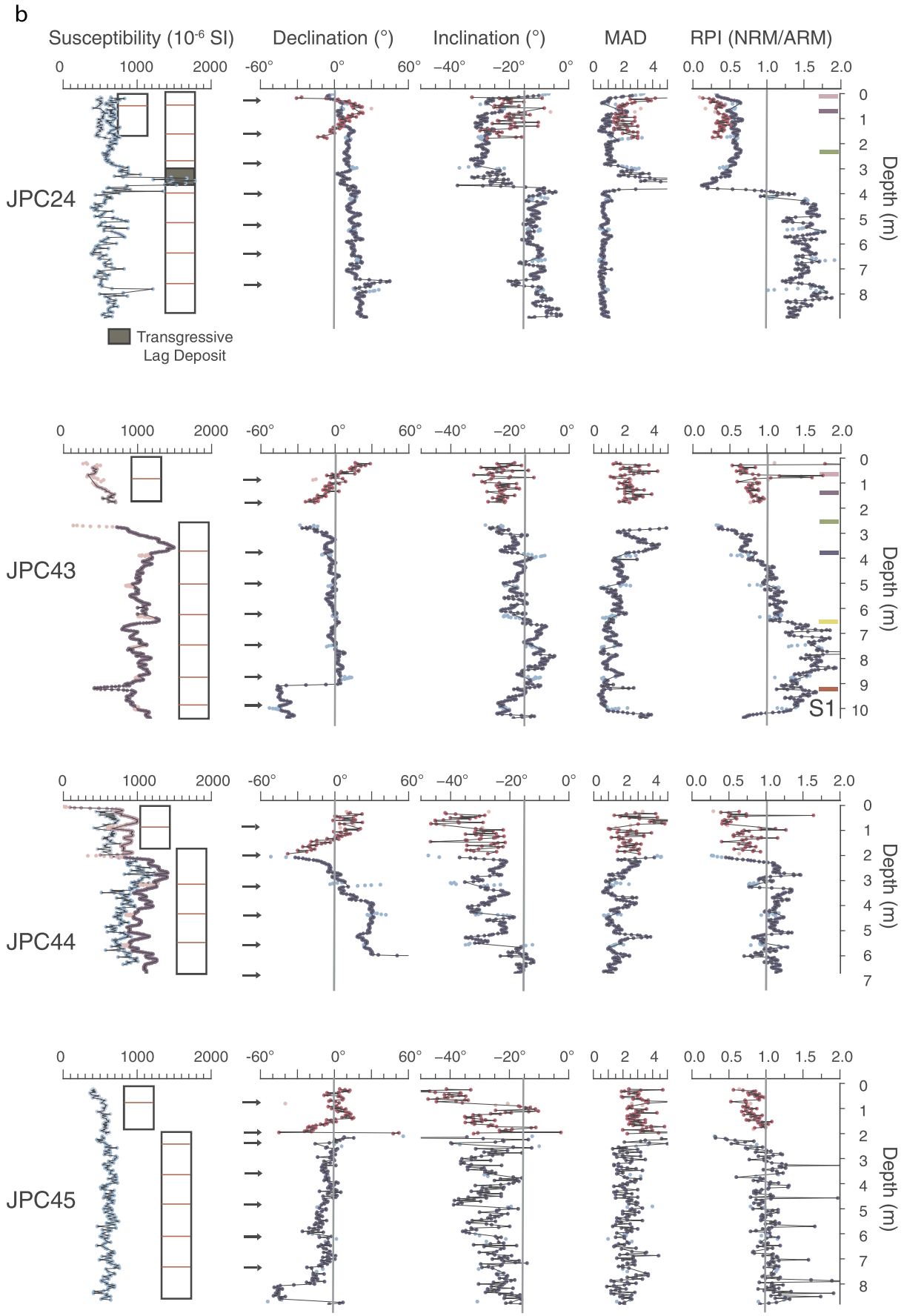

Fig. 6. (*continued*)

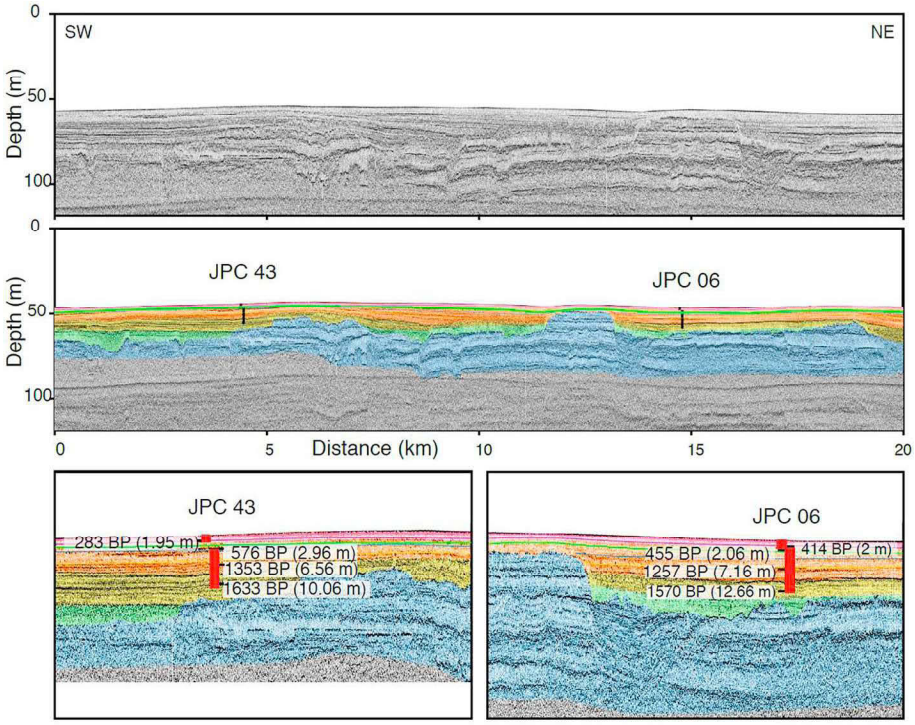

Fig. 7. The top panel shows an uninterpreted Knudsen seismic profile. The middle panel shows the same profile with interpretations of the sediment packages (colors, see text). Seismic reflectors have been traced between cores JPC06 and JPC43 and are shown in thin colored lines. The bottom panel shows the two cores in detail with the reflectors and calibrated radiocarbon ages marked. "a" indicates the calibrated radiocarbon age, and "d" indicates the depth below seafloor of that radiocarbon age. (For interpretation of the references to color in this figure legend, the reader is referred to the web version of this article.)

sections where there were large (> 30°) abrupt changes in relative declination. They are visible in JPC43, JPC44 and JPC45, occur at three different times (1800 BP, 400 BP and 300 BP), and do not swing in the same direction in all three cores (Fig. 11). Cores JPC43 and JPC44 were measured with both U-channels and discrete samples across the swing in declination to verify that there was no error in the sampling or measurement of the U-channel. These swings in declination occurred in the middle of sections, away from any deformation evident at section ends. The MAD values and inclination values at these points do not deviate from the typical values, there are no visible changes in lithology, and the near vertical alignment of the minimum susceptibility axes give us confidence that these cores represented an environment that has been relatively undisturbed since deposition. These swings occur near the bottoms of the cores but are well above the depth where flow-in occurs, which can be observed visibly and is also readily identified by the off-vertical minimum susceptibility axis with high MAD values.

It is also difficult to conceive how half a section of core could be rotated in the process of sectioning, capping, or splitting the cores, since the clay is very cohesive and there was no visible evidence of such a

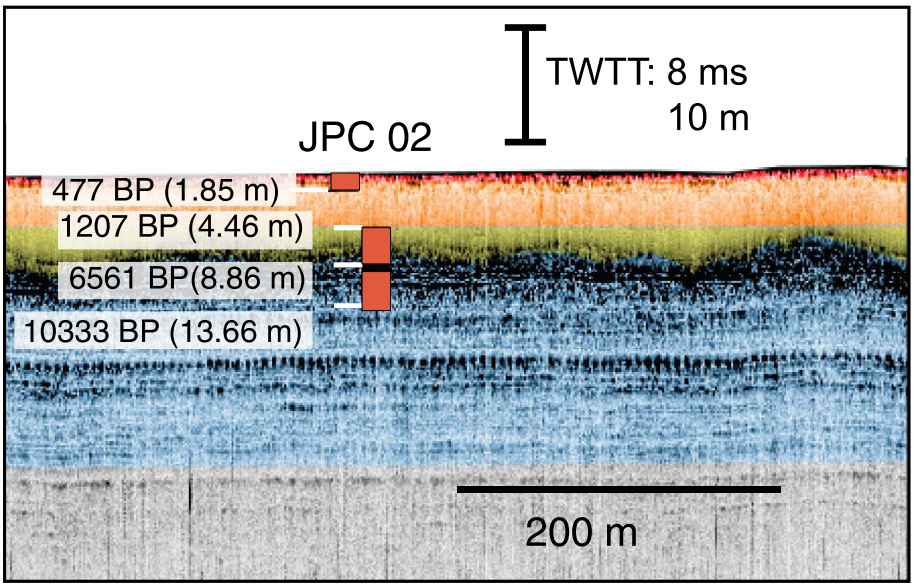

Fig. 8. An interpreted seismic CHIRP profile for JPC02. Depths of radiocarbon ages, and calibrated ages in years BP are noted. The ^{14}C age of the trigger core sample is labeled "tc", "d" corresponds to the depth in the core of the radiocarbon age, and "a" corresponds to the ^{14}C age of the sediment in the piston. Yellow, Orange and Red packages in the Holocene clinothem consist of fine-grained mud, Green (too thin to show in the seismic profile) represents transgressive deposits composed of shell fragments and sand in a mud matrix and the older relict Blue clinothem. (For interpretation of the references to color in this figure legend, the reader is referred to the web version of this article.)

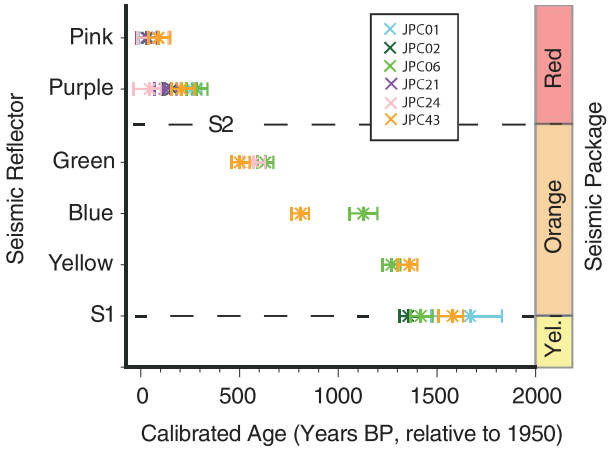

Fig. 9. Apparent ages of seismic reflectors in each core, determined using calibrated radiocarbon dates above and below each reflector. Reflectors were identified within the Orange and Red seismic packages and additionally at the S1 surface (Slingerland et al., 2008a) separating the Yellow and Orange packages. S2 represents the surface separating the Orange and Red seismic packages. Star represents best age, and the whiskers represent maximum and minimum estimates on the age from the 1-sigma error on the radiocarbon dates. (For interpretation of the references to color in this figure legend, the reader is referred to the web version of this article.)

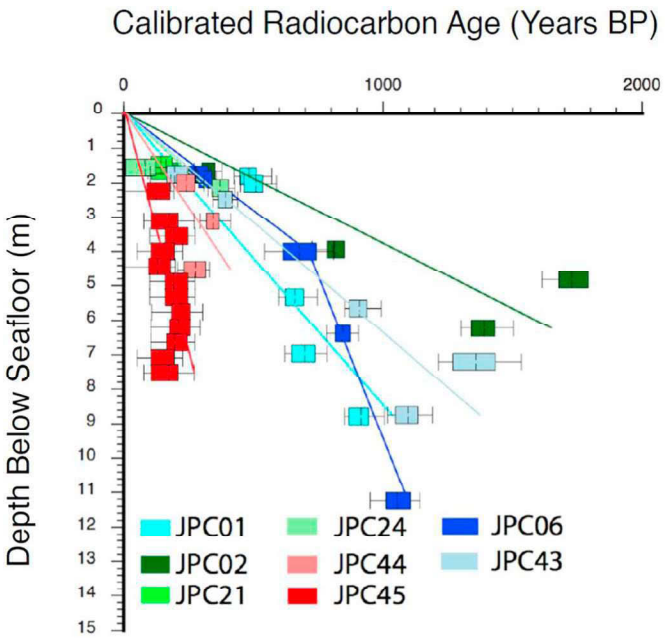

Fig. 10. Calibrated radiocarbon ages and best fit line with one sigma (box) and 2 sigma (whisker) error bars plotted against depth.

rotation, that is no break or gap in the core was observed. Another possibility is that these declination shifts represent a slump or fluid mud flow. The cores are far enough apart and sedimentation in the area is varied enough that these three declination shifts could represent three different events, with no requirement that the event be present in all cores, but with a slump or mudflow there should be some difference in magnetic fabric – more triaxial instead of oblate fabric, a change in the direction of Kmax, or an off-vertical minimum axis (Schwehr et al., 2006). In all three cores, there is no distinct change in fabric type or systematic variation in Kmax.

A final possibility is that these swings represent true changes in the geomagnetic field. This seems unlikely as the swings trend in different directions, are not visible in every core, and are not accompanied by a significant increase or decrease in intensity or inclination. Additionally, the rate at which these apparent shifts occur are significantly faster than anything predicted by gufm/IGRF at the location or even at similar latitudes. Rates predicted by these models are on the order of 0.05° per year - a factor of twenty smaller than the directional change observed (> 50° of declination change over less than fifty years). Although we don't believe these represent true changes in the field, with a sufficient number of records, these large swings will have minimal effect on the resulting stack. Similar observations of abrupt changes in declination have been made previously (Barletta et al., 2010a, 2010b) with no viable explanation.

6. Conclusions

We presented a high resolution paleosecular variation and relative paleointensity stacked record from a set of cores collected in the Gulf of Papua. Dating was performed on all cores using AMS radiocarbon, and showed that sedimentation was up to 500 cm/kyr in some locations, but also extremely variable. This high sedimentation rate allows for identification of features on short time scales. The main magnetic carrier was determined to be PSD (titano)magnetite, and the similar character of demagnetization curves for NRM and ARM as well as minimal grain size variation suggest that ARM is a suitable normalizer when determining paleointensity.

Our results from dating both the bottoms of the trigger cores and tops of the piston cores allowed us to determine the offset of the piston core with tools other than matching density or susceptibility. This approach revealed that in many cores there was no overlap of the two and the piston core had penetrated the seafloor much deeper than the trigger core before acquiring sediment.

Seismic data collected in the area were able to place additional constraints on the offsets calculated for the piston cores using sedimentation rates and correlation of reflectors between cores is consistent with the radiocarbon dates (Fig. 8). Seismic data is very useful for aiding in paleomagnetic correlation, but it should be employed with caution because of the three dimensional variability of depositional packages. Correlations often break down across large distances where the assumption that a horizon is an isochron is less likely to be valid. Regardless of which parameter one chooses to aid in correlation of cores, there should be careful consideration before making the assumption that variations are time equivalent.

There are many challenges involved with separating true variations in the magnetic field from uncertainties in the coring process and from complexities in depositional environment. To create an ideal stack and minimize uncertainties, there is a need for multiple cores from the same site (meaning identical geographic coordinates) and multiple sets from a small region. An excellent way to sample a site is with a companion gravity core, which will ensure there is no data gap (from piston core over penetration), and will provide a means of validating data from the upper portion of the piston core. A second piston core at a site would be labor and time intensive, but would allow one to isolate variations due to the coring process from variations due to the environment. Multiple radiocarbon dates from sets of cores in the region should be employed to establish an age model and highlight any regional variations in sedimentation.

Despite these limitations, our stacked record from this region shows a steepening in inclination over the past 2000 years and an eastward trend in declination, which is in good agreement with other nearby

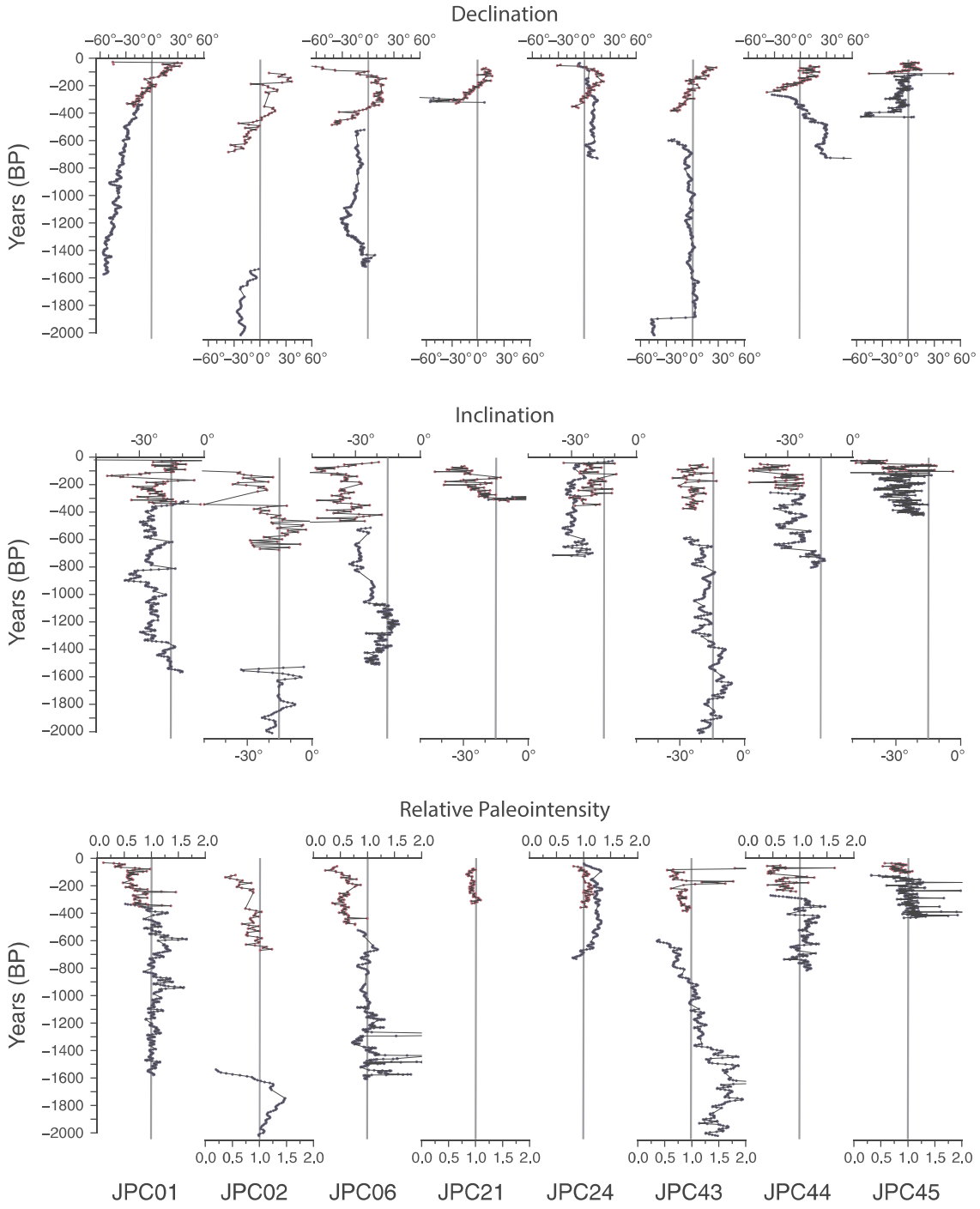

Fig. 11. Relative declination, inclination, and relative paleointensity for each core. Trigger core is shown in deep pink and piston core is shown in blue. GAD inclination predicted at this site is shown with a grey line. (For interpretation of the references to color in this figure legend, the reader is referred to the web version of this article.)

results, including ODP Hole 1202B (Richter et al., 2006), and Lake Pounui (Turner and Lillis, 1994). The stacked record based on these cores is inconsistent with both CALS3k and pfm9k. The poor agreement with these models is not unexpected since the models are poorly constrained by data in this region. This agreement with nearby records gives a good indication that the marine sediments in the Gulf of Papua are a reliable recorder of the magnetic field, but more data from the region would help improve Holocene field models.

Supplementary data to this article can be found online at https://doi.org/10.1016/j.margeo.2018.11.014.

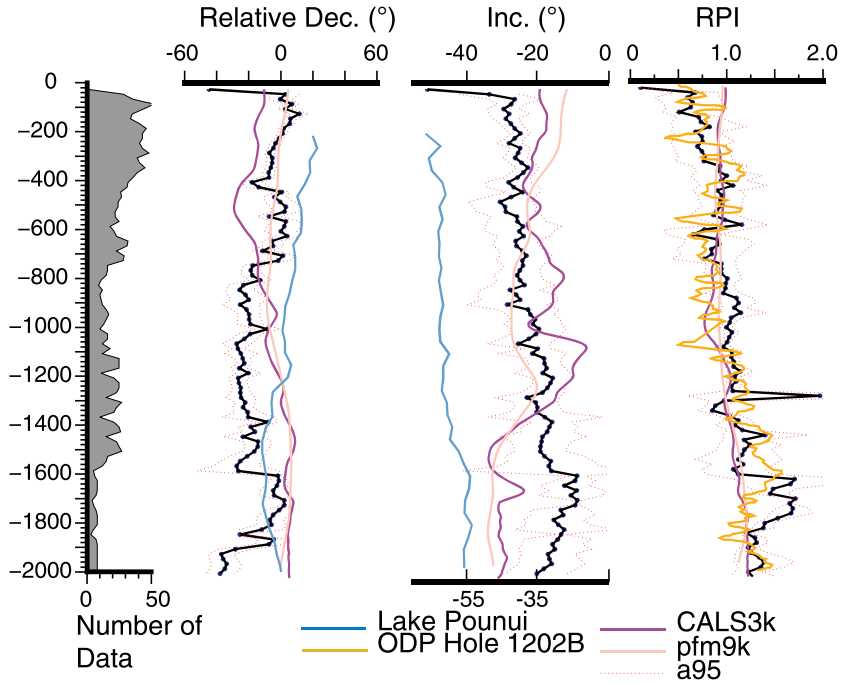

Fig. 12. Stacked record using 20 year age bins. Fisher mean is plotted in blue for declination and inclination with alpha 95 confidence interval (dotted red) and RPI mean (blue) and standard deviation (dotted red). Grey bars at left indicate number of points used to average. Model predictions from CALS3k and pfm9k are shown in purple and light pink. Results from Lake Pounui (Turner and Lillis, 1994), with inclination scale shown at bottom, and ODP Hole 1202B (Richter et al., 2006) are plotted for comparison. (For interpretation of the references to color in this figure legend, the reader is referred to the web version of this article.)

Acknowledgements

Core acquisition was funded by the National Science Foundation award 0305699 under the MARGINS Source to Sink program. We also would like to thank the crew of the R/V Melville, and Alex Hangsterfer who helped with cores. Carl Richter kindly provided us with data from ODP 1202.

References

Ali, M., Oda, H., Hayashida, A., Takemura, K., Torii, M., 1999. Holocene paleomagnetic secular variation at Lake Biwa, central Japan. Geophys. J. Int. 136, 218–228.

Barletta, F., St-Onge, G., Channell, J.E.T., Rochon, A., Polyak, L., Darby, D., 2008. High-resolution paleomagnetic secular variation and relative paleointensity records from the western Canadian Arctic: implication for Holocene stratigraphy and geomagnetic field behaviour. Can. J. Earth Sci. 45, 1265–1281. https://doi.org/10.1139/E08-039.

Barletta, F., St-Onge, G., Channell, J.E.T., Rochon, A., 2010a. Dating of Holocene western Canadian Arctic sediments by matching paleomagnetic secular variation to a geomagnetic field model. Quat. Sci. Rev. 29, 2315–2324. https://doi.org/10.1016/j.quascirev.2010.05.035.

Barletta, F., St-Onge, G., Stoner, J.S., Lajeunesse, P., Locat, J., 2010b. A high-resolution Holocene paleomagnetic secular variation and relative paleointensity stack from eastern Canada. Earth Planet. Sci. Lett. 298, 162–174. https://doi.org/10.1016/j.epsl.2010.07.038.

Barton, C.E., McElhinny, M.W., 1981. A 10 000 yr geomagnetic secular variation record from three Australian maars. Geophys. J. R. Astron. Soc. 67, 465–485. https://doi.org/10.1111/j.1365-246X.1981.tb02761.x.

Bol'shakov, V.A., Dolotov, A., 2012. Magnetic properties of greigite in the Late Pleistocene sediments of the North Caspian. Izv. Phys. Solid Earth 48, 516–531. https://doi.org/10.1134/S1069351312050023.

Brachfeld, S.A., Banerjee, S.K., 2000. A new high-resolution geomagnetic relative paleointensity record for the North American Holocene: a comparison of sedimentary and absolute intensity data. J. Geophys. Res. 105, 821. https://doi.org/10.1029/1999JB900365.

Brachfeld, S., Acton, G.D., Guyodo, Y., Banerjee, S.K., 2000. High-resolution paleomagnetic records from Holocene sediments from the Palmer Deep, Western Antartic Peninsula. Earth Planet. Sci. Lett. 181, 429–441. https://doi.org/10.1016/S0012-821X(00)00211-9.

Brachfeld, S., Barletta, F., St-Onge, G., Darby, D., Ortiz, J.D., 2009. Impact of diagenesis on the environmental magnetic record from a Holocene sedimentary sequence from the Chukchi-Alaskan margin, Arctic Ocean. Glob. Planet. Chang. 68, 100–114. https://doi.org/10.1016/j.gloplacha.2009.03.023.

Buckley, D.E., MacKinnon, W.G., Cranston, R.E., Christian, H.A., 1994. Problems with piston core sampling: mechanical and geochemical diagnosis. Mar. Geol. 117, 95–106. https://doi.org/10.1016/0025-3227(94)90008-6.

Bullard, E.C., Freedman, C., Gellman, H., Nixon, J., 1950. The westward drift of the Earth's magnetic field. Philos. Trans. R. Soc. Lond. A 243 (859), 67–92.

Burr, G.S., Beck, J.W., Correge, T., Cabioch, G., Taylor, F.W., Donahue, D.J., 2009. Modern and Pleistocene reservoir ages inferred from south. Radiocarbon 51, 319–335.

Channell, J.E.T., Xuan, C., Hodell, D.A., 2009. Stacking paleointensity and oxygen isotope data for the last 1.5 Myr (PISO-1500). Earth Planet. Sci. Lett. 283, 14–23. https://doi.org/10.1016/j.epsl.2009.03.012.

Chappell, J., Polach, H.A., 1976. Holocene sea-level change and coral-reef growth at Huon Peninsula, Papua New Guinea. Geol. Soc. Am. Bull. 87 (2), 235–240.

Christl, M., Strobl, C., Mangini, A., 2003. Beryllium-10 in deep-sea sediments: a tracer for the Earth's magnetic field intensity during the last 200,000 years. Quat. Sci. Rev. 22, 725–739. https://doi.org/10.1016/S0277-3791(02)00195-6.

Clement, B.M., Kent, D.V., 1987. Short polarity intervals within the Matuyama: transitional field records from hydraulic piston cored sediments from the North Atlantic. Earth Planet. Sci. Lett. 81, 253–264. https://doi.org/10.1016/0012-821X(87)90161-0.

Constable, C.G., 1985. Eastern Australian geomagnetic field intensity over the past 14,000 years. Geophys. J. R. Astron. Soc. 81, 121–130. https://doi.org/10.1111/j.1365-246X.1985.tb01354.x.

Constable, C.G., McElhinny, M.W., 1985. Holocene geomagnetic secular variation records from north-eastern Australian lake sediments. Geophys. J. R. Astron. Soc. 81, 103–120. https://doi.org/10.1111/j.1365-246X.1985.tb01353.x.

Constable, C.G., Tauxe, L., 1987. Paleointensity of the pelagic realm: marine sediment data compared with archeomagnetic and lake sediments records. Geophys. J. R. Astron. Soc. 90, 43–59.

Day, R., Fuller, M., Schmidt, V.A., 1977. Hysteresis properties of titanomagnetites: grain-size and compositional dependence. Phys. Earth Planet. Inter. 13, 260–267. https://doi.org/10.1016/0031-9201(77)90108-X.

Dumberry, M., Finlay, C.C., 2007. Eastward and westward drift of the Earth's magnetic field for the last three millennia. Earth Planet. Sci. Lett. 254, 146–157. https://doi.org/10.1016/j.epsl.2006.11.026.

Frank, U., Nowaczyk, N.R., Negendank, J.F.W., 2007. Rock magnetism of greigite bearing sediments from the Dead Sea, Israel. Geophys. J. Int. 168, 921–934. https://doi.org/10.1111/j.1365-246X.2006.03273.x.

Gee, J.S., Tauxe, L., Constable, C., 2008. AMSSpin: a LabVIEW program for measuring the anisotropy of magnetic susceptibility with the Kappabridge KLY-4S. Geochem. Geophys. Geosyst. 9. https://doi.org/10.1029/2008GC001976.

Gillespie, R., Polach, H.A., 1979. 1979: the suitability of marine shells for radiocarbon dating of Australian prehistory. In: Berger, R., Suess, H.E. (Eds.), Radiocarbon Dating.

International ^{14}C Conference 9, Proceedings. University of California Press, pp. 404–421.
Gogorza, C.S.G., Sinito, A.M., Lirio, J.M., Nuez, H., Chaparro, M., Vilas, J.F., 2002. Paleosecular variations 0–19,000 years recorded by sediments from Escondido Lake (Argentina). Phys. Earth Planet. Inter. 133, 35–55. https://doi.org/10.1016/S0031-9201(02)00086-9.
Haberzettl, T., St-Onge, G., Behling, H., Kirleis, W., 2013. Evaluating Late Holocene radiocarbon-based chronologies by matching palaeomagnetic secular variations to geomagnetic field models: an example from Lake Kalimpaa (Sulawesi, Indonesia). Geol. Soc. Lond. Spec. Publ. 373 (1), 245–259. https://doi.org/10.1144/SP373.10.
Harris, P.T., 1994. Incised valleys and backstepping deltaic deposits in a foreland-basin setting, Torres Strait and Gulf of Papua, Australia. In: Incised-Valley Syst. Orig. Sediment. Seq. SEPM, Spec. Publ. 51. pp. 45–62.
Harris, P.T., Baker, E.K., Cole, A.R., Short, S.A., 1993. A preliminary study of sedimentation in the tidally dominated Fly River Delta, Gulf of Papua. Cont. Shelf Res. 13, 441–472. https://doi.org/10.1016/0278-4343(93)90060-B.
Harris, P.T., Pattiaratchi, C.B., Keene, J.B., Dalrymple, R.W., Gardner, J.W., Barker, E.K., Cole, A.R., Mitchell, D., Gibbs, P., Schroeder, W.W., 1996. Late Quaternary deltaic and carbonate sedimentation in the Gulf of Papua Foreland Basin: response to sea-level change. SEPM J. Sediment. Res. 66, 801–819. https://doi.org/10.1306/D426840F-2B26-11D7-8648000102C1865D.
Harrison, C.G.A., Somayajulu, B.L.K., 1966. Behavior of the Earth's magnetic field during a reversal. Nature 212, 1193–1195. https://doi.org/10.1038/2121193a0.
Jackson, A., Jonkers, A.R.T., Walker, M.R., 2000. Four centuries of geomagnetic secular variation from historical records. Philos. Trans. R. Soc. A Math. Phys. Eng. Sci. 358, 957–990. https://doi.org/10.1098/rsta.2000.0569.
Jackson, M., Bowles, J.A., Lascu, I., Solheid, P., 2010. Deconvolution of u channel magnetometer data: experimental study of accuracy, resolution, and stability of different inversion methods. Geochem. Geophys. Geosyst. 11, 1–21. https://doi.org/10.1029/2009GC002991.
Johnstone, E.A.C., 2012. Geophysical Constraints on Sediment Dispersal Systems. University of California, San Diego.
Keigwin, L.D., Klotsko, S., Zhao, N., Reilly, B., Giosan, L., Driscoll, N.W., 2018. Deglacial Floods in the Beaufort Sea Preceded Younger Dryas Cooling. https://doi.org/10.1038/s41561-018-0169-6.
King, J., Banerjee, S.K., Marvin, J., Özdemir, Ö., 1982. A comparison of different magnetic methods for determining the relative grain size of magnetite in natural materials: some results from lake sediments. Earth Planet. Sci. Lett. 59, 404–419. https://doi.org/10.1016/0012-821X(82)90142-X.
King, J.W., Banerjee, S.K., Marvin, J., 1983. A new rock-magnetic approach to selecting sediments for geomagnetic paleointensity studies: application to paleointensity for the last 4000 years. J. Geophys. Res. Solid Earth 88 (B7), 5911–5921.
Kirschvink, J.L., 1980. The least-square line and plane and the analysis of paleomagnetic data. Geophys. J. R. Astron. Soc. 62, 699–718.
Korte, M., Constable, C.G., 2005. The geomagnetic dipole moment over the last 7000 years—new results from a global model. Earth Planet. Sci. Lett. 236, 348–358. https://doi.org/10.1016/j.epsl.2004.12.031.
Korte, M., Constable, C., 2011. Improving geomagnetic field reconstructions for 0–3 ka. Phys. Earth Planet. Inter. 188, 247–259. https://doi.org/10.1016/j.pepi.2011.06.017.
Lean, C.M.B., McCave, I.N., 1998. Glacial to interglacial mineral magnetic and palaeoceanographic changes at Chatham Rise, SW Pacific Ocean. Earth Planet. Sci. Lett. 163, 247–260. https://doi.org/10.1016/S0012-821X(98)00191-5.
Levi, S., Banerjee, S.K., 1976. On the possibility of obtaining relative paleointensities from lake sediments. Earth Planet. Sci. Lett. 29, 219–226. https://doi.org/10.1016/0012-821X(76)90042-X.
Lisé-Pronovost, A., St-Onge, G., Brachfeld, S., Barletta, F., Darby, D., 2009. Paleomagnetic constraints on the Holocene stratigraphy of the Arctic Alaskan margin. Glob. Planet. Chang. 68, 85–99. https://doi.org/10.1016/j.gloplacha.2009.03.015.
Lund, S.P., Stott, L., Schwartz, M., Thunell, R., Chen, A., 2006. Holocene paleomagnetic secular variation records from the western Equatorial Pacific Ocean. Earth Planet. Sci. Lett. 246, 381–392. https://doi.org/10.1016/j.epsl.2006.03.056.
Lund, S., Platzman, E., Johnson, T., 2016. Full-vector paleomagnetic secular variation records from latest quaternary sediments of Lake Malawi (10.0°S, 34.3°E). Quat. Sci. Rev. 144, 16–27. https://doi.org/10.1016/j.quascirev.2016.03.010.
Lunne, T., Long, M., 2006. Review of long seabed samplers and criteria for new sampler design. Mar. Geol. 226, 145–165. https://doi.org/10.1016/j.margeo.2005.07.014.
Mackereth, F.J.H., 1971. On the variation in direction of the horizontal component of remanent magnetisation in lake sediments. Earth Planet. Sci. Lett. 12, 332–338. https://doi.org/10.1016/0012-821X(71)90219-6.
Maloney, Jillian M., Noble, Paula J., Driscoll, Neal W., Kent, Graham M., Smith, Shane B., Schmauder, Gretchen C., Babcock, Jeffrey M., et al., 2013. Paleoseismic history of the Fallen Leaf segment of the West Tahoe–Dollar Point fault reconstructed from slide deposits in the Lake Tahoe Basin, California-Nevada. Geosphere 9 (4), 1065–1090.
McGregor, H.V., Gagan, M.K., McCulloch, M.T., Hodge, E., Mortimer, G., 2008. Mid-Holocene variability in the marine ^{14}C reservoir age for northern coastal Papua New Guinea. Quat. Geochronol. 3, 213–225. https://doi.org/10.1016/j.quageo.2007.11.002.
Milliman, J.D., 1993. Production and accumulation of calcium carbonate in the ocean: budget of a nonsteady state. Glob. Biogeochem. Cycles 7 (4), 927–957.
Milliman, J.D., 1995. Sediment discharge to the ocean from small mountainous rivers: the New Guinea example. Geo-Mar. Lett. 15, 127–133. https://doi.org/10.1007/BF01204453.
Milliman, J.D., Farnsworth, K.L., Albertin, C.S., 1999. Flux and fate of fluvial sediments leaving large islands in the East Indies. J. Sea Res. 41, 97–107. https://doi.org/10.1016/S1385-1101(98)00040-9.
Nagata, T., 1965. Main characteristics of recent geomagnetic secular variation. J. Geomagn. Geoelectr. 17 (3–4), 263–276.
Nelson, D.M., Tréguer, P., Brzezinski, M.A., Leynaert, A., Quéguiner, B., 1995. Production and dissolution of biogenic silica in the ocean: revised global estimates, comparison with regional data and relationship to biogenic sedimentation. Glob. Biogeochem. Cycles 9 (3), 359–372.
Nilsson, A., Holme, R., Korte, M., Suttie, N., Hill, M., 2014. Reconstructing Holocene geomagnetic field variation: new methods, models and implications. Geophys. J. Int. 198, 229–248. https://doi.org/10.1093/gji/ggu120.
Ohneiser, C., Acton, G., Channell, J.E.T., Wilson, G.S., Yamamoto, Y., Yamazaki, T., 2013. A middle Miocene relative paleointensity record from the Equatorial Pacific. Earth Planet. Sci. Lett. 374, 227–238. https://doi.org/10.1016/j.epsl.2013.04.038.
Opdyke, N.D., Henry, K.W., 1969. A test of the dipole hypothesis. Earth Planet. Sci. Lett. 6 (2), 139–151.
Peck, J.A., King, J.W., Colman, S.M., Kravchinsky, V.A., 1996. An 84-kyr paleomagnetic record from the sediments of Lake Baikal, Siberia. J. Geophys. Res. Solid Earth 101, 11365–11385.
Reimer, P.J., Bard, E., Bayliss, A., Beck, J.W., Blackwell, P.G., Bronk Ramsey, C., Buck, C.E., Cheng, H., Edwards, R.L., Friedrich, M., Grootes, P.M., Guilderson, T.P., Haflidason, H., Hajdas, I., Hatté, C., Heaton, T.J., Hoffmann, D.L., Hogg, A.G., Hughen, K.A., Kaiser, K.F., Kromer, B., Manning, S.W., Niu, M., Reimer, R.W., Richards, D.A., Scott, E.M., Southon, J.R., Staff, R.A., Turney, C.S.M., van der Plicht, J., 2013. IntCal13 and Marine13 radiocarbon age calibration curves 0–50,000 years cal BP. Radiocarbon 55, 1869–1887. https://doi.org/10.2458/azu_js_rc.55.16947.
Rhodes, E.G., Polach, H.A., Thom, B.G., Wilson, S.R., 1980. Age structure of Holocene coastal sediments: Gulf of Carpentaria, Australia. Radiocarbon 22, 718–727.
Richter, C., Venuti, A., Verosub, K.L., Wei, K.Y., 2006. Variations of the geomagnetic field during the Holocene: relative paleointensity and inclination record from the West Pacific (ODP Hole 1202B). Phys. Earth Planet. Inter. 156, 179–193. https://doi.org/10.1016/j.pepi.2005.08.006.
Roberts, A.P., 1995. Magnetic properties of sedimentary freigite (Fe_3S_4). Earth Planet. Sci. Lett. 134, 227–236.
Ron, H., Nowaczyk, N.R., Frank, U., Schwab, M.J., Naumann, R., Striewski, B., Agnon, A., 2007. Greigite detected as dominating remanence carrier in Late Pleistocene sediments, Lisan formation, from Lake Kinneret (Sea of Galilee), Israel. Geophys. J. Int. 170, 117–131. https://doi.org/10.1111/j.1365-246X.2007.03425.x.
Sadler, P.M., 1981. Sediment accumulation rates and the completeness of stratigraphic sections. J. Geol. 89 (5), 569–584.
Sakai, H., Nomura, S., Horii, M., Kashiwaya, K., Tanaka, A., Kawai, T., Kravchinsky, V., Peck, J., King, J., 2000. Paleomagnetic and rock-magnetic studies on Lake Baikal sediments: BDP 96 borehole at Academician Ridge. Lake Baikal. In: A Mirror Time Sp. Underst. Glob. Chang. Process, pp. 35–52.
Schwehr, K., Tauxe, L., Driscoll, N., Lee, H., 2006. Detecting compaction disequilibrium with anisotropy of magnetic susceptibility. Geochem. Geophys. Geosyst. 7 (11).
Slingerland, R., Driscoll, N.W., Milliman, J.D., Miller, S.R., Johnstone, E.A., 2008a. Anatomy and growth of a Holocene clinothem in the Gulf of Papua. J. Geophys. Res. Earth Surf. 113, 1–16. https://doi.org/10.1029/2006JF000628.
Slingerland, R., Selover, R.W., Ogston, A.S., Keen, T.R., Driscoll, N.W., Milliman, J.D., 2008b. Building the Holocene clinothem in the Gulf of Papua: an ocean circulation study. J. Geophys. Res. Earth Surf. 113, 1–17. https://doi.org/10.1029/2006JF000680.
Snowball, I.F., 1997. Gyroremanent magnetization and the magnetic properties of greigite-bearing clays in southern Sweden. Geophys. J. Int. 129, 624–636. https://doi.org/10.1111/j.1365-246X.1997.tb04498.x.
Stoner, J.S., St-Onge, G., 2007. Chapter three magnetic stratigraphy in paleoceanography: reversals, excursions, paleointensity, and secular variation. Dev. Mar. Geol. 1, 99–138. https://doi.org/10.1016/S1572-5480(07)01008-1.
Stoner, J.S., Laj, C., Channell, J.E.T., Kissel, C., 2002. South Atlantic and North Atlantic geomagnetic paleointensity stacks\r(0–80 ka): implications for inter-hemispheric correlation. Quat. Sci. Rev. 21, 1141–1151.
Stoner, J.S., Jennings, A., Kristjánsdóttir, G.B., Dunhill, G., Andrews, J.T., Hardardóttir, J., 2007. A paleomagnetic approach toward refining Holocene radiocarbon-based chronologies: paleoceanographic records from the North Iceland (MD99-2269) and East Greenland (MD99-2322) margins. Paleoceanography 22, 1–23. https://doi.org/10.1029/2006PA001285.
Stuiver, M., Reimer, P.J., 1993. Extended ^{14}C data base and revised CALIB 3.0 ^{14}C age calibration program. Radiocarbon 35 (1), 215–230.
Tauxe, L., 1993. Sedimentary records of relative paleointensity of the geomagnetic field: theory and practice. Rev. Geophys. 31, 319–354.
Turner, G.M., Lillis, D.A., 1994. A palaeomagnetic secular variation record for New Zealand during the past 2500 years. Phys. Earth Planet. Inter. 83, 265–282. https://doi.org/10.1016/0031-9201(94)90093-0.
Turner, G.M., Howarth, J.D., de Gelder, G.I.N.O., Fitzsimons, S.J., 2015. A new high-resolution record of Holocene geomagnetic secular variation from New Zealand. Earth Planet. Sci. Lett. 430, 296–307. https://doi.org/10.1016/j.epsl.2015.08.021.

Valet, J.-P., Meynadier, L., Guyodo, Y., 2005. Geomagnetic dipole strength and reversal rate over the past two million years. Nature 435, 802–805. https://doi.org/10.1038/nature03674.

Verosub, K.L., Mehringer, P.J., Waterstraat, P., 1986. Holocene secular variation in Western North America: paleomagnetic record from fish lake, Harney county, Oregon. J. Geophys. Res. Solid Earth 91 (B3), 3609–3623.

Vestine, E.H., 1953. On variations of the geomagnetic field, fluid motions, and the rate of the earth's rotation. J. Geophys. Res. 58 (2), 127–145.

Walsh, J.P., Nittrouer, C.A., Palinkas, C.M., Ogston, A.S., Sternberg, R.W., Brunskill, G.J., 2004. Clinoform mechanics in the Gulf of Papua, New Guinea. Cont. Shelf Res. 24, 2487–2510. https://doi.org/10.1016/j.csr.2004.07.019.

Wardinski, I., Korte, M., 2008. The evolution of the core-surface flow over the last seven thousands years. J. Geophys. Res. Solid Earth 113, 1–16. https://doi.org/10.1029/2007JB005024.

Wei, E.A., Driscoll, N.W., Slingerland, R.L., 2018. Oceanographic currents, differential subsidence, and physiography control three-dimensional clinothem growth in the Gulf of Papua, Papua New Guinea. Mar. Geol. 407, 164–180.

Wu, H., Zhao, X., Shi, M., Zhang, S., Li, H., Yang, T., 2014. A 23 Myr magnetostratigraphic time framework for Site 1148, ODP Leg 184 in South China Sea and its geological implications. Mar. Pet. Geol. 58, 749–759. https://doi.org/10.1016/j.marpetgeo.2014.01.003.

Xuan, C., Channell, J.E.T., 2009. UPmag: MATLAB software for viewing and processing u channel or other pass-through paleomagnetic data. Geochem. Geophys. Geosyst. 10, 1–12. https://doi.org/10.1029/2009GC002584.

Yamamoto, Y., Yamazaki, T., Kanamatsu, T., Ioka, N., Mishima, T., 2007. Relative paleointensity stack during the last 250 kyr in the Northwest Pacific. J. Geophys. Res. Solid Earth 112. https://doi.org/10.1029/2006JB004477.

Zhou, Lei, Kyte, Frank T., 1992. Sedimentation history of the South Pacific pelagic clay province over the last 85 million years inferred from the geochemistry of Deep Sea Drilling Project Hole 596. Paleoceanography 7 (4), 441–465.

Ziegler, L.B., Constable, C.G., Johnson, C.L., Tauxe, L., 2011. PADM2M: a penalized maximum likelihood model of the 0–2 Ma palaeomagnetic axial dipole moment. Geophys. J. Int. 184, 1069–1089. https://doi.org/10.1111/j.1365-246X.2010.04905.x.